

Physics potential of neutrino oscillation experiment with a far detector in Oki Island along the T2K baseline

Kaoru Hagiwara^{1,2}, Takayuki Kiwanami^{2*},
Naotoshi Okamura^{3†}, and Ken-ichi Senda^{1‡}

¹ *KEK Theory Center, Tsukuba, 305-0801, Japan*

² *Sokendai, (The Graduate University for Advanced Studies), Tsukuba, 305-0801, Japan*

³ *Faculty of Engineering, University of Yamanashi, Kofu, Yamanashi, 400-8511, Japan*

Abstract

Oki Island is located between Japan and Korea along the Tokai-To-Kamioka (T2K) baseline. The distance from J-PARC to Oki Island is about 653km, which is twice that of the T2K experiment ($L = 295\text{km}$). When the off-axis angle of the neutrino beam from J-PARC is 3.0° (2.0°) at Super-Kamiokande (SK), the off-axis beam (OAB) with 1.4° (0.6°) reaches at Oki Island. We examine physics case of placing a far detector in Oki Island during the T2K experimental period. We estimate the matter density profile along the Tokai-to-Oki baseline by using recent seismological measurements. For a detector of 100 kton fiducial volume and 2.5×10^{21} POT (protons on target) exposure for both ν_μ and $\bar{\nu}_\mu$ beams, we find that the mass hierarchy pattern can be distinguished at 3σ level if $\sin^2 2\theta_{\text{RCT}} \equiv 4|U_{e3}|^2(1 - |U_{e3}|^2) \gtrsim 0.09$, by observing the electron-like CCQE (Charged-Current Quasi Elastic) events. The CP phase in the Maki-Nakagawa-Sakata lepton flavor mixing matrix, δ_{MNS} , can be constrained with $\pm 20^\circ$. As a reference, we repeat the same analysis by placing the same detector in Korea at $L = 1000\text{ km}$ and $\text{OAB} = 0.5^\circ$ (T2KK) and also by placing it at the SK site (T2K₁₂₂). The Tokai-to-Kamioka-OKI (T2KO) sensitivity to the mass hierarchy is about 1/3 (in $\Delta\chi_{\text{min}}^2$) of T2KK, while the sensitivity to the phase δ_{MNS} is similar between T2KO and T2KK. The T2K₁₂₂ option has almost no sensitivity to the mass hierarchy, and cannot measure the CP phase except when $\delta_{\text{MNS}} \sim -90^\circ$ (90°) for the normal (inverted) hierarchy.

*Present address : PLP Division, SHINKO ELECTRIC INDUSTRIES CO., LTD, Nagano, 381-0103, Japan.

†e-mail : nokamura@yamanashi.ac.jp

‡e-mail : senda@post.kek.jp

1 Introduction

Since the neutrino oscillation was first observed at Super-Kamiokande (SK) [1], many experiments have measured the physics parameters of the neutrino oscillation [2]-[12].

Some of these experiments observe the survival probability of ν_μ and $\bar{\nu}_\mu$ which are generated in the atmosphere by the cosmic ray [2]. Accelerator based long baseline experiments [3, 4, 5] also measure the ν_μ survival probability. From the combined results of these experiments [2]-[5], the mass-squared difference and the mixing angle are obtained as

$$\sin^2 2\theta_{\text{ATM}} > 0.90 \quad (90\% \text{C.L.}), \quad (1a)$$

$$|\delta m_{\text{ATM}}^2| = (2.35_{-0.08}^{+0.11}) \times 10^{-3} \text{eV}^2. \quad (1b)$$

The sign of the mass-squared difference, eq. (1b), cannot be determined from these experiments. The SK collaboration also reported that the atmospheric neutrinos oscillate into active neutrinos [6].

The combined results of the solar neutrino observations [7, 8], which measure the survival probability of ν_e from the sun, and the KamLAND experiment [9], which measure the $\bar{\nu}_e$ flux from the reactors at distances of a few 100 km, find

$$\sin^2 2\theta_{\text{SOL}} = 0.852_{-0.026}^{+0.024}, \quad (2a)$$

$$\delta m_{\text{SOL}}^2 = (7.50_{-0.20}^{+0.19}) \times 10^{-5} \text{eV}^2, \quad (2b)$$

where the sign of mass-squared difference has been determined by the matter effect inside the sun [13]. The SNO experiment determined that ν_e from the sun changes into active neutrinos [8].

For the reactor experiments, which measure the survival probability of $\bar{\nu}_e$ from the reactor at distances of $L \sim O(1)$ km [10, 11], the CHOOZ experiment observed no signal, giving

$$\sin^2 2\theta_{\text{RCT}} < 0.17, \quad (3a)$$

$$\text{for } |\delta m_{\text{RCT}}^2| = 2.35 \times 10^{-3} \text{eV}^2, \quad (3b)$$

at the 90% confidence level [10]. More recently, the T2K collaboration reported several $\nu_\mu \rightarrow \nu_e$ appearance candidate events giving

$$0.03 (0.04) < \sin^2 2\theta_{\text{RCT}} < 0.28 (0.34) \quad (4)$$

for $\sin^2 \theta_{23} = 0.5$ and $\delta_{\text{MNS}} = 0^\circ$ with the normal (inverted) hierarchy at the 90% confidence level [14]. The MINOS collaboration reported

$$\sin^2 2\theta_{\text{RCT}} = 0.041_{-0.031}^{+0.047} (0.079_{-0.053}^{+0.071}) \quad (5)$$

also for $\sin^2 \theta_{23} = 0.5$ and $\delta_{\text{MNS}} = 0^\circ$ with the normal (inverted) hierarchy [15]. The Double CHOOZ collaboration, which is one of the new reactor experiments, found hints of reactor electron anti-neutrino disappearance consistent with neutrino oscillation and reported

$$\sin^2 2\theta_{\text{RCT}} = 0.086 \pm 0.041 (\text{stat.}) \pm 0.030 (\text{syst.}) \quad (6)$$

from analyzing both the rate of the prompt positrons and their energy spectrum [16]. Recently another new reactor experiment, the DayaBay experiment [17], announced that they have measured the neutrino mixing angle as

$$\sin^2 2\theta_{\text{RCT}} = 0.092 \pm 0.016 \text{ (stat.)} \pm 0.005 \text{ (syst.)}, \quad (7)$$

which is more than 5σ away from zero. The RENO collaboration, which also measure the reactor $\bar{\nu}_e$ survival probability, shows the evidence of the non-zero mixing angle;

$$\sin^2 2\theta_{\text{RCT}} = 0.113 \pm 0.013 \text{ (stat.)} \pm 0.019 \text{ (syst.)}, \quad (8)$$

from a rate-only analysis, which is 4.9σ away from zero.

Since the MiniBooNE experiment [12] did not confirm the LSND observation of rapid $\bar{\nu}_\mu \rightarrow \bar{\nu}_e$ oscillation [18], there is no clear indication of experimental data which suggests more than three neutrinos. Therefore the $\nu_\mu \rightarrow \nu_e$ appearance analysis of T2K [14] and MINOS[15] presented above assume the 3 neutrino model, with the 3×3 flavor mixing, the MNS (Maki-Nakagawa-Sakata) matrix [19]

$$\begin{pmatrix} \nu_e \\ \nu_\mu \\ \nu_\tau \end{pmatrix} = \begin{pmatrix} U_{e1} & U_{e2} & U_{e3} \\ U_{\mu1} & U_{\mu2} & U_{\mu3} \\ U_{\tau1} & U_{\tau2} & U_{\tau3} \end{pmatrix} \begin{pmatrix} \nu_1 \\ \nu_2 \\ \nu_3 \end{pmatrix}, \quad (9)$$

relating the weak interaction eigenstates $(\nu_e, \nu_\mu, \nu_\tau)$ and the mass eigenstate ν_i with the mass m_i ($i = 1, 2, 3$). The mass-squared differences that dictate the neutrino oscillation phase are then identified as

$$\delta m_{\text{ATM}}^2 = \delta m_{\text{RCT}}^2 = m_3^2 - m_1^2, \quad (10a)$$

$$\delta m_{\text{SOL}}^2 = m_2^2 - m_1^2, \quad (10b)$$

where only the magnitude of the larger mass-squared difference, $m_3^2 - m_1^2$ is determined in eq. (1b). The $m_3^2 > m_1^2$ case is called normal, while $m_3^2 < m_1^2$ case is called inverted neutrino mass hierarchy. With a good approximation [20], the three independent mixing angles of the MNS matrix can be related to the oscillation amplitudes in eqs. (1a), (2a), and $\sin^2 2\theta_{\text{RCT}}$ in eqs. (3a), (4) to (7), with the MNS matrix elements $U_{\alpha i}$:

$$\sin \theta_{\text{ATM}} = U_{\mu 3} = \sin \theta_{23} \cos \theta_{13}, \quad (11a)$$

$$\sin \theta_{\text{RCT}} = |U_{e3}| = \sin \theta_{13}, \quad (11b)$$

$$\sin 2\theta_{\text{SOL}} = 2U_{e1}U_{e2} = \sin 2\theta_{12} \cos^2 \theta_{13}. \quad (11c)$$

In the last equations, the defining region of the three mixing angles $\theta_{ij} = \theta_{ji}$ can be chosen as $0 \leq \theta_{12}, \theta_{13}, \theta_{23} \leq \pi/2$ [21], which is consistent with the convention of non-negative U_{e1} and U_{e2} [22]. The argument of U_{e3} gives the CP phase of the MNS matrix,

$$\delta_{\text{MNS}} = -\arg U_{e3}. \quad (12)$$

Even after θ_{RCT} , the smallest of the three mixing angles, is measured by the accelerator based long baseline experiments [14, 15] and the reactor experiments [16, 17, 23], three unknowns remain in the 3 neutrino model, which are the sign of the larger mass-squared differences, normal ($m_3^2 - m_1^2 > 0$) or inverted ($m_3^2 - m_1^2 < 0$), the leptonic CP phase (δ_{MNS}), and the sign of $\sin^2 \theta_{\text{ATM}} - 0.5$ if its magnitude differs from zero significantly. The main purpose of the next generation neutrino oscillation experiments is to determine these three unknown parameters of the three neutrino model.

The accelerator based long baseline neutrino oscillation experiment with two-detectors for one-beam, such as Tokai-to-Kamioka-and-Korea (T2KK) experiment [24]-[30], is one of the promising experiments for measuring all the three unknowns. When one measures the neutrino energy (E_ν) and the magnitude of the ν_e appearance probability at significantly different baseline lengths, the degeneracy between the sign of the larger mass-squared difference and the CP phase can be resolved [26]-[30], since they affect the magnitude of the ν_e appearance probability and the neutrino energy at the first oscillation maximum differently at the two baseline lengths. Once the mass hierarchy and the CP phase are determined, the sign of $\sin^2 \theta_{\text{ATM}} - 0.5$ can be determined [28] since the $\nu_\mu \rightarrow \nu_e$ oscillation probability is proportional to $\sin^2 \theta_{\text{ATM}} \sin^2 \theta_{\text{RCT}}$.

In the previous works [26]-[30], physics impacts of the T2KK experiment have been studied systematically, and the following observations have been made: If a 100 kton water Čerenkov detector is placed in Korea at $L = 1000$ km observing the 0.5° off-axis beam (OAB) during the T2K exposure time of 5×10^{21} POT (protons on target), the mass hierarchy can be resolved at 3σ level for $\sin^2 2\theta_{\text{RCT}} \gtrsim 0.05$ (0.06) when the hierarchy is normal (inverted), and the CP phase can be constrained uniquely, by measuring the CCQE (Charged-Current Quasi Elastic) events [26, 27]. The sign of $\sin^2 \theta_{\text{ATM}} - 0.5$ can also be determined for $|\sin^2 \theta_{\text{ATM}} - 0.5| = 0.1$ with 3σ level, if $\sin^2 2\theta_{\text{RCT}} > 0.12$ for the normal hierarchy [28]. When we take into account the smearing of reconstructed neutrino energy due to finite detector resolution and the Fermi motion of target nucleons, resonance production, and the neutral current (NC) π^0 production background to the ν_e appearance signal, it is found that the mass hierarchy pattern can still be determined at 3σ level for $\sin^2 2\theta_{\text{RCT}} \gtrsim 0.08$ (0.09) when the hierarchy is normal (inverted), but the CP phase can no longer be established at 3σ level with 5×10^{21} POT ν_μ exposure [29]. In Ref.[30], matter distribution profile along the T2K and Tokai-to-Korea baselines have been studied, and merits of splitting the total exposure time into half ν_μ and half $\bar{\nu}_\mu$ beam have been reported. Studies on the impacts of the neutrino energy smearing and the NC π^0 background for the $\bar{\nu}_\mu \rightarrow \bar{\nu}_e$ oscillation measurements are in progress [31].

Oki Island* is placed between Japan and Korea along the T2K baseline and inside Japanese territory. The distance from J-PARC to Oki Island is about $L = 653$ km which is about two times longer than that of the T2K experiment ($L = 295$ km). In Fig. 1, we show the surface map of the T2K, T2KO (Tokai-to-Kamioka-and-Oki), and T2KK experiments,

*This island is sometimes called “Oki-no-Shima”, because “Shima” means an “Island”, “no” is “in”, and “Oki” means the “Offing”; an island in the offing, or an offshore island.



Figure 1: The surface map of the T2K, T2KO, and T2KK experiment. The yellow blobs show the center of the neutrino beam for the T2K experiment at the sea level, where the number in the white box is the off-axis angle at SK.

in which the red lines denote the baselines for each experiment and the yellow blobs show the center of the neutrino beam from J-PARC at the sea level, when the off-axis angle at SK is 2° , 2.5° , and 3° . The authors of Ref.[32] consider the physics performance of a 100 kton Liquid Argon Time Projection Chamber placed at Oki Island. In Ref.[33], the authors studied the Oki Island site from the geological, geographic and infrastructure points of view for the possibility to construct a large detector. They conclude that Oki Island is one of the good candidate sites for a large detector.

In this paper, we study the physics potential of a 100 kton water Čerenkov detector placed in Oki Island instead of Korea during the T2K experimental period, by using exactly the same setting assumed for the T2KK experiment in Ref.[30], except for the location of the detector. This allows us to compare the physics capability of the two proposals on the same footing. Since we do assume in this analysis that the $\nu_\mu \rightarrow \nu_\mu, \nu_e$ CCQE events can be distinguished from the background, our results should equally be applied for a more advanced Liquid Argon detector [32].

This article is organized as follows. In the next section, we briefly review neutrino oscillation in the matter and give useful approximation formula for $\nu_\mu \rightarrow \nu_\mu, \nu_e$ and $\bar{\nu}_\mu \rightarrow \bar{\nu}_\mu, \bar{\nu}_e$ oscillation probabilities. In section 3, we show the matter profile between J-PARC and Oki Island by using recent seismological measurements and give relations between the off-axis angle observable at Oki and that at SK. The expected numbers of $\nu_\mu \rightarrow \nu_\mu, \nu_e$ ($\bar{\nu}_\mu \rightarrow \bar{\nu}_\mu, \bar{\nu}_e$) CCQE events at the far (Oki) and the near (SK) detectors are shown for typical parameters in section 4. In section 5, we present the χ^2 function with which we estimate the statistical sensitivity of the T2KO and T2KK experiments on the mass hierarchy and the CP phase. In section 6, we show the results on the mass hierarchy determination of the T2KO experiment and compare it with T2KK, and also with T2K₁₂₂ where the 100 kton detector is placed in the Kamioka site making the total fiducial volume 122 kton at $L = 295$ km. In section 7, we show the CP phase sensitivity of T2KO, T2KK,

and T2K₁₂₂ experiments. We summarize our findings in the last section.

2 Neutrino oscillation in the matter

In long baseline neutrino oscillation experiments, neutrinos from the accelerator interact coherently with electrons and nucleons by charged and neutral current interactions. These coherent interactions make an additional potential in the effective Hamiltonian [13]. Because the potential from the neutral current interactions are flavor-blind, it does not affect the neutrino oscillation probability in the three neutrino model. On the other hand, the charged-current interactions contribute only to the effective potential of ν_e and $\bar{\nu}_e$. The neutrino oscillation probabilities hence depend on the matter density profile along the baseline. Detailed studies on the matter distribution dependence of the oscillation probabilities for the T2K and T2KK experiments are found in Ref. [30]. In this exploratory analysis, we compare the physics capability of the T2KO, T2KK, and T2K experiments by using the average matter density along the baselines which is found to approximate the matter effects rather accurately [30].

The Hamiltonian of a neutrino propagating in the matter is then expressed as

$$H = \frac{1}{2E} \left[U \begin{pmatrix} 0 & & \\ & \delta m_{12}^2 & \\ & & \delta m_{13}^2 \end{pmatrix} U^\dagger + \begin{pmatrix} \bar{a}_0 & & \\ & 0 & \\ & & 0 \end{pmatrix} \right], \quad (13a)$$

$$= \frac{1}{2E} \tilde{U} \begin{pmatrix} \lambda_1 & & \\ & \lambda_2 & \\ & & \lambda_3 \end{pmatrix} \tilde{U}^\dagger, \quad (13b)$$

on the flavor space $(\nu_e, \nu_\mu, \nu_\tau)^T$, with $\delta m_{ij}^2 \equiv m_j^2 - m_i^2$, where

$$\bar{a}_0 = 2\sqrt{2}G_F E_\nu n_e \simeq 7.56 \times 10^{-5} \text{eV}^2 \left(\frac{\bar{\rho}}{\text{g/cm}^3} \right) \left(\frac{E_\nu}{\text{GeV}} \right) \quad (14)$$

gives the matter effect with the electron number density n_e , which is approximated by the average matter density $\bar{\rho}$ (g/cm³) along the baseline. By using the solution of eq. (13b), the oscillation probability that an initial flavor eigenstate ν_α is observed as a flavor eigenstate ν_β after traveling a distance L along the baseline is

$$P_{\nu_\alpha \rightarrow \nu_\beta} = \left| \langle \nu_\beta | \exp \left(-i \int_0^L H dx \right) | \nu_\alpha \rangle \right|^2, \quad (15a)$$

$$= \delta_{\alpha\beta} - 4 \sum_{i < j} \text{Re}(\tilde{U}_{\alpha i}^* \tilde{U}_{\beta i} \tilde{U}_{\alpha j} \tilde{U}_{\beta j}^*) \sin^2 \frac{\tilde{\Delta}_{ij}}{2} + 2 \sum_{i < j} \text{Im}(\tilde{U}_{\alpha i}^* \tilde{U}_{\beta i} \tilde{U}_{\alpha j} \tilde{U}_{\beta j}^*) \sin \tilde{\Delta}_{ij}, \quad (15b)$$

where

$$\tilde{\Delta}_{ij} \equiv \frac{\lambda_j - \lambda_i}{2E_\nu} L. \quad (16)$$

All our numerical results are based on eq. (15). However, we find the following analytic approximations [26, 30] useful for understanding the reason why and how the one-beam two-detectors long baseline experiments such as T2KK [26]-[30] and T2KO, with a far detector in Oki Island, can determine the neutrino mass hierarchy and the CP phase simultaneously. They are obtained by expanding the oscillation probabilities in terms of the three small parameters; the matter effects, which is small at energies below a few GeV around the earth crust for $\bar{\rho} \sim 3 \text{ g/cm}^3$ and $L \lesssim 1000 \text{ km}$, the oscillation phase $\Delta_{12} \equiv \delta m_{12}^2 L / 2E_\nu$, which is also small ($\sim \pi/30$) near the first oscillation maximum, $|\Delta_{13}| \sim \pi$, and the mixing factor $|U_{e3}|^2 = \sin^2 \theta_{\text{RCT}}$, eq. (11b), which is about 1/40 from the recent reactor measurements eqs. (7) and (8).

The ν_μ survival probability can then be approximated as

$$P_{\nu_\mu \rightarrow \nu_\mu} = 1 - \sin^2 2\theta_{\text{ATM}} (1 + A^\mu) \sin^2 \left(\frac{\Delta_{13} + B^\mu}{2} \right), \quad (17)$$

around the first maximum of the main oscillation phase

$$\Delta_{13} \equiv \delta m_{13}^2 \frac{L}{2E_\nu} = \frac{m_3^2 - m_1^2}{2E_\nu} L, \quad (18)$$

with

$$A^\mu = -\frac{a_0 L}{\Delta_{13} E_\nu} (1 - \tan^2 \theta_{\text{ATM}}) \sin^2 \theta_{\text{RCT}}, \quad (19a)$$

$$B^\mu = \frac{a_0 L}{2E_\nu} (1 - \tan^2 \theta_{\text{ATM}}) \sin^2 \theta_{\text{RCT}} - \Delta_{12} (\cos^2 \theta_{\text{SOL}} + \tan^2 \theta_{\text{ATM}} \sin^2 \theta_{\text{SOL}} \sin^2 \theta_{\text{RCT}} - \tan \theta_{\text{ATM}} \sin 2\theta_{\text{SOL}} \sin \theta_{\text{RCT}} \cos \delta_{\text{MNS}}) \quad (19b)$$

We find that the above formula reproduce the survival probability with 1% accuracy throughout the parameter range explored in this analysis, which covers all the three neutrino model parameters in the 3σ allowed range of the present measurements eqs. (1)-(8), for the neutrino energies $400 \text{ MeV} < E_\nu < 4 \text{ GeV}$ (for $\nu_\mu, \bar{\nu}_\mu$), and for the baseline lengths $295 \text{ km} < L < 1200 \text{ km}$, except where the probability is very small, ($P_{\nu_\mu \rightarrow \nu_\mu} \lesssim 10^{-5}$) [27, 30]. The matter effects are proportional to the term

$$\frac{a_0 L}{2E_\nu} \simeq 0.58 \left(\frac{\bar{\rho}}{3 \text{ g/cm}^3} \right) \left(\frac{L}{1000 \text{ km}} \right) \quad (20)$$

and it appears with the opposite sign both in the amplitude correction term A^μ eq. (19a) where $\Delta_{13} = |\Delta_{13}|$ for the normal while $\Delta_{13} = -|\Delta_{13}|$ for the inverted hierarchy, and also in the phase shift in eq. (17), where $|\Delta_{13} + B^\mu| = \pi + B^\mu$ for the normal, $\pi - B^\mu$ for the inverted hierarchy around the oscillation maximum $|\Delta_{13}| \simeq \pi$. Nevertheless, the effect is too small to be observed in the near future because the term $1 - \tan^2 \theta_{\text{ATM}}$ is bounded as

$$0.48 > 1 - \tan^2 \theta_{\text{ATM}} > -0.92 \quad (21)$$

at 90% C.L. from eq. (1a), and because both A^μ and B^μ are proportional to the product of the two small parameters, the matter effect term of $a_0 L / 2E_\nu$ and $\sin^2 \theta_{\text{RCT}}$. The coefficient

of $\cos \delta_{\text{MNS}}$ in B^μ is also small, only 1% of the main oscillation phase $|\Delta_{13}|$. In other words, the ν_μ survival probability is very insensitive to the unknown parameters of the three neutrino model, and hence can be used to measure $\sin^2 \theta_{\text{ATM}}$ and $|\delta m_{23}^2|$ accurately.

Under the same conditions that give eq. (17) for the ν_μ survival probability, the ν_e appearance probability can be approximated as [30]

$$P_{\nu_\mu \rightarrow \nu_e} = 4 \sin^2 \theta_{\text{ATM}} \sin^2 \theta_{\text{RCT}} \left\{ (1 + A^e) \sin^2 \left(\frac{\Delta_{13}}{2} \right) + \frac{B^e}{2} \sin \Delta_{13} \right\} + C^e, \quad (22)$$

where we retain both linear and quadratic terms of Δ_{12} and a_0 . The analytic expressions for the correction terms A^e , B^e and C^e are found in Ref.[30]. For our semi-quantitative discussion below, the following numerical estimates [30] for $\sin^2 2\theta_{\text{ATM}} = 1$ and $\sin^2 2\theta_{\text{SOL}} = 0.852$ suffice:

$$A^e \simeq 0.37 \frac{\bar{\rho}}{3\text{g/cm}^3} \frac{L}{1000\text{km}} \frac{\pi}{\Delta_{13}} \left(1 - \frac{\sin^2 2\theta_{\text{RCT}}}{2} \right) - 0.29 \left| \frac{\Delta_{13}}{\pi} \right| \sqrt{\frac{0.1}{\sin^2 2\theta_{\text{RCT}}}} \left[1 + 0.18 \frac{\bar{\rho}}{3\text{g/cm}^3} \frac{L}{1000\text{km}} \frac{\pi}{\Delta_{13}} \right] \sin \delta_{\text{MNS}}, \quad (23a)$$

$$B^e \simeq -0.58 \frac{\bar{\rho}}{3\text{g/cm}^3} \frac{L}{1000\text{km}} \left(1 - \frac{\sin^2 2\theta_{\text{RCT}}}{2} \right) + 0.30 \left| \frac{\Delta_{13}}{\pi} \right| \left[\sqrt{\frac{0.1}{\sin^2 2\theta_{\text{RCT}}}} \cos \delta_{\text{MNS}} - 0.11 \right] \left[1 + 0.18 \frac{\bar{\rho}}{3\text{g/cm}^3} \frac{L}{1000\text{km}} \frac{\pi}{\Delta_{13}} \right]. \quad (23b)$$

The term C^e is relevant only when the $\nu_\mu \rightarrow \nu_e$ oscillation probability is very small [30].

The first term in A^e in eq. (23a) is sensitive not only to the matter effect but also to the mass hierarchy pattern, since $\Delta_{13} \sim \pi$ for the normal while $\Delta_{13} \sim -\pi$ for the inverted hierarchy around the oscillation maximum. For the normal (inverted) hierarchy, the magnitude of the $\nu_\mu \rightarrow \nu_e$ transition probability is enhanced (suppressed) by about 10% at Kamioka, 24% at Oki Island, and 37% at $L \sim 1000$ km in Korea, around the first oscillation maximum, $|\Delta_{13}| \sim \pi$. When L/E_ν is fixed at $|\Delta_{13}| \sim \pi$, the difference between the two hierarchy cases grows with L , because the matter effect grows with E_ν . Within the allowed range of the model parameters, the difference of the A^e between SK and a far detector at Oki or Korea becomes

$$A_{\text{peak}}^e(L = 653\text{km}) - A_{\text{peak}}^e(L = 295\text{km}) \simeq \pm 0.13, \quad (24a)$$

$$A_{\text{peak}}^e(L \sim 1000\text{km}) - A_{\text{peak}}^e(L = 295\text{km}) \simeq \pm 0.26, \quad (24b)$$

where the upper sign corresponds to the normal, and the lower sign for the inverted hierarchy. The hierarchy pattern can hence be determined by comparing $P_{\nu_\mu \rightarrow \nu_e}$ near the oscillation maximum $|\Delta_{13}| \simeq \pi$ at two vastly different baseline lengths [26]-[30], *independently* of the sign and magnitude of $\sin \delta_{\text{MNS}}$.

In eq. (23b), it is also found that the first term in B^e , which shifts the oscillation phase from $|\Delta_{13}|$ to $|\Delta_{13} + B^e| = |\Delta_{13}| \pm B^e$, is also sensitive to the mass hierarchy pattern. As

in the case for A^e , the difference in B^e between SK and a far detectors is found to be

$$B_{\text{peak}}^e(L = 653\text{km}) - B_{\text{peak}}^e(L = 295\text{km}) \simeq \mp 0.10, \quad (25\text{a})$$

$$B_{\text{peak}}^e(L \sim 1000\text{km}) - B_{\text{peak}}^e(L = 295\text{km}) \simeq \mp 0.20, \quad (25\text{b})$$

where the upper sign is for the normal, and the lower sign for the inverted hierarchy. This implies that the mass hierarchy pattern can also be discriminated by measuring the neutrino energy of the first oscillation maximum at two different baseline lengths. As in the case of the oscillation amplitude above, this determination can be made independent of the unknown $\cos \delta_{\text{MNS}}$ terms since they cancel in the differences, eq. (25).

Once the sign of Δ_{13} is fixed by the terms linear in $\bar{\rho}$, the terms linear in Δ_{12} , which appear as those proportional to $|\Delta_{13}| \sim 30\Delta_{12}$ in eq. (23), allow us to constrain $\sin \delta_{\text{MNS}}$ via the amplitude A^e , and $\cos \delta_{\text{MNS}}$ via the phase shift B^e . Therefore, δ_{MNS} can be measured uniquely once the mass hierarchy pattern is determined. From the above discussions, we understand qualitatively why the mass hierarchy as well as both $\sin \delta_{\text{MNS}}$ and $\cos \delta_{\text{MNS}}$ can be determined uniquely by observing the $\nu_\mu \rightarrow \nu_e$ oscillation probability around the first oscillation maximum at two vastly different baseline lengths. Therefore, in order to take advantage of this very efficient mechanism to determine all the main unknowns of the three neutrino model, one should arrange for high neutrino flux both at near and far detectors around the first oscillation maximum which appears at the same energy-to-baseline-length ratio,

$$\left| \frac{\Delta_{13}}{\pi} \right| = \frac{(L/295\text{km})}{(E_\nu/0.55\text{GeV})} = \frac{(L/653\text{km})}{(E_\nu/1.22\text{GeV})} = \frac{(L/1000\text{km})}{(E_\nu/1.86\text{GeV})} \quad (26)$$

for $|\delta m_{13}^2| = 2.35 \times 10^{-3} \text{eV}^2$; eq. (1b). This observation led to the T2KK proposal of choosing the 3° off-axis beam ($E_\nu^{\text{peak}} \sim 0.55\text{GeV}$) at SK and $\sim 0.5^\circ$ off-axis beam ($E_\nu^{\text{peak}} \sim 1.1\text{GeV}$) at $L \sim 1000\text{km}$ [26, 27]. Since the baseline length of $L \sim 653\text{km}$ to Oki Island is about a factor of two longer than $L \sim 295\text{km}$ for T2K, we may also expect that a beam with smaller off-axis angle at Oki Island will enhance its physics capability; see, however, discussions in section 6.

The oscillation probabilities for the anti-neutrino, $P(\bar{\nu}_\alpha \rightarrow \bar{\nu}_\beta)$, are obtained from the expressions for $P(\nu_\alpha \rightarrow \nu_\beta)$ by reversing the sign of the matter effect term, ($\bar{\rho} \rightarrow -\bar{\rho}$), and that of δ_{MNS} , ($\delta_{\text{MNS}} \rightarrow -\delta_{\text{MNS}}$). The differences in the shift terms A^e and B^e for $\nu_\mu \rightarrow \nu_e$ and \bar{A}^e and \bar{B}^e for $\bar{\nu}_\mu \rightarrow \bar{\nu}_e$ oscillation probabilities are, respectively,

$$A^e - \bar{A}^e = \pm 0.74 \frac{\bar{\rho}}{3\text{g/cm}^3} \frac{L}{1000\text{km}} \left| \frac{\pi}{\Delta_{13}} \right| \left(1 - \frac{\sin^2 2\theta_{\text{RCT}}}{2} \right) - 0.58 \left| \frac{\Delta_{13}}{\pi} \right| \sqrt{\frac{0.1}{\sin^2 2\theta_{\text{RCT}}}} \sin \delta_{\text{MNS}}, \quad (27\text{a})$$

$$B^e - \bar{B}^e = -1.16 \frac{\bar{\rho}}{3\text{g/cm}^3} \frac{L}{1000\text{km}} \times \left[1 - \frac{\sin^2 2\theta_{\text{RCT}}}{2} \mp 0.093 \left(\sqrt{\frac{0.1}{\sin^2 2\theta_{\text{RCT}}}} \cos \delta_{\text{MNS}} - 0.11 \right) \right], \quad (27\text{b})$$

where the upper sign should be taken for the normal and the lower sign for the inverted hierarchy. From eq. (27a), the difference of the amplitude between ν_e and $\bar{\nu}_e$ appearance probability grows with the baseline length with the opposite sign for the normal and inverted hierarchies. The dependence on $\sin \delta_{\text{MNS}}$ is also strong since A^e and \bar{A}^e changes in the opposite direction when we vary $\sin \delta_{\text{MNS}}$. The phase-shift term B^e and \bar{B}^e also change sign in the opposite direction for the normal and inverted hierarchies, whose sign is independent of $\cos \delta_{\text{MNS}}$ because of the smallness of the $\cos \delta_{\text{MNS}}$ dependence in eq. (27b). By the same token, the use of both ν_μ and $\bar{\nu}_\mu$ beams does not improve significantly the measurement of $\cos \delta_{\text{MNS}}$. Because these sign changes occur independently of the L -dependence of the oscillation probabilities, the physics potential of the T2KO experiment will be improved by dividing the total exposure time to neutrino and anti-neutrino beams just as in T2KK [30].

It is worth noting here that all the formalism presented in this section should be useful for studying physics potential of T2K plus NOvA [34], whose baseline length of $L \simeq 810$ km lies between those of Tokai to Oki Island ($L \simeq 653$ km) and to Korea ($L \gtrsim 1000$ km).

3 T2K, T2KO, and T2KK baselines

In this section, we study the matter profile along the baselines between J-PARC and Kamioka, Oki Island, and Korea by referring to recent seismological measurements [35]-[42]. We also show the relation between the off-axis angles at SK and Oki Island, and the beam profiles for the relevant off-axis angles [43].

3.1 Matter profile along the baselines

Because Oki Island is placed just at the middle point between SK and the east shore of Korea along the T2K beam, as shown in Fig. 1, the cross section view of the T2K, T2KO, and T2KK experiments along the baselines can be shown on one frame as in Fig. 2. The horizontal axis of Fig. 2 gives the distance from J-PARC along the arc of the earth surface and the vertical axis denotes the depth below the sea level. Three curves show the baselines from the J-PARC to SK ($L = 295\text{Km}$), Oki Island ($L = 653\text{km}$) and to the Korean east shore at $L = 1000\text{km}$. The numbers in the white boxes are the average matter density of the layer in units of g/cm^3 .

If we assume that the matter density in each layer of the earth crust as shown in Fig. 2 has the value equals to the quoted average, we can estimate the average matter density $\bar{\rho}$ along the three baselines:

$$\bar{\rho}_{\text{T2K}} = 2.60 \text{ g}/\text{cm}^3, \quad (28a)$$

$$\bar{\rho}_{\text{T2Oki}} = 2.75 \text{ g}/\text{cm}^3, \quad (28b)$$

$$\bar{\rho}_{\text{T2Kr}(1000\text{km})} = 2.90 \text{ g}/\text{cm}^3. \quad (28c)$$

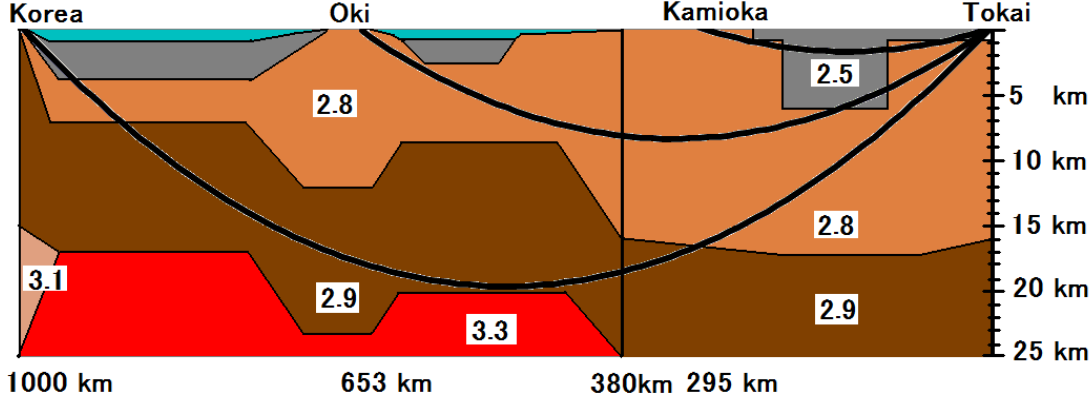


Figure 2: The cross section view of the T2K, T2KO, and T2KK experiments along the baselines, which are shown by the three curves. The horizontal scale gives the distance from J-PARC along the arc of the earth surface and the vertical scale measures the depth of the baseline below the sea level. The numbers in the white boxes are the average matter density in units of g/cm^3 [35]-[42].

The error of these average density can be estimated from the uncertainty of the matter density in each region and the location of the boundary of each layer. They are measured by using the velocity of the seismic wave in most geophysical researches. From the uncertainty in the correlation between the matter density and the measured p -wave sound velocity [42, 30], we adopt 6% overall error for the matter density. Small fluctuation in the matter density in each layer of the earth crust does not affect the neutrino oscillation probabilities significantly, because the contribution from the higher Fourier modes of the matter density distribution is strongly suppressed [44, 30]. The locations of the boundaries are measured rather accurately from the reflection point of the seismic wave. From Fig. 2, we find that the neutrino beam for the Tokai-to-Oki baseline goes through the upper crust layer with $\bar{\rho} = 2.8\text{g}/\text{cm}^3$, except when it crosses Fossa Magna filled with sediment. The uncertainty of the boundary depth between the sediment layer and the upper crust is only a few hundred meters. The error from the uncertainty of the boundary depth can hence be safely neglected for the T2KO experiment. The traveling distance in the mantle and the crust depends on the depth of the boundary between the lower crust and the upper mantle for the T2KK experiment. The average matter density is sensitive to the boundary location for the baseline of $L \sim 1000$ km, because the baseline almost touches the mantle as can be seen from Fig. 2. The resulting uncertainty has been estimated and is found to be significantly smaller than the 6% overall uncertainty [30]. We therefore use the average matter density along each baseline given in eq. (28) to estimate the oscillation probability and assign its overall uncertainty of 6% in this study.

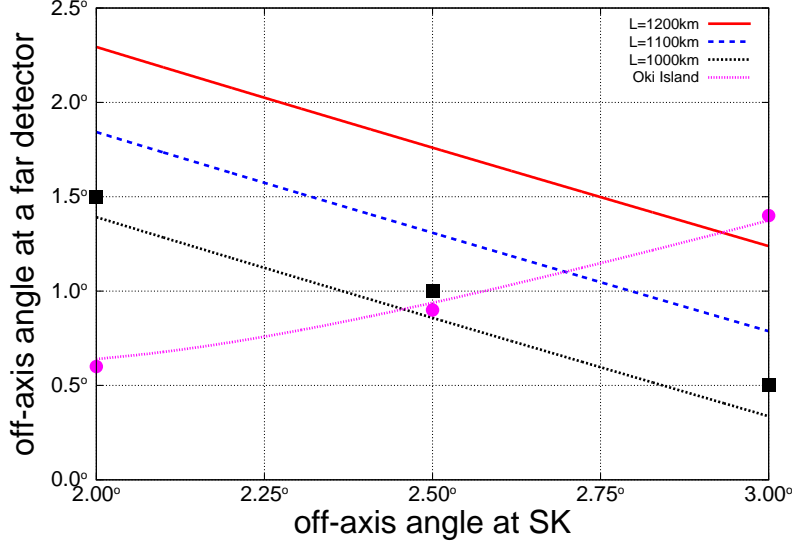


Figure 3: The relation among the off-axis angles at SK, Oki Island, and at a far detector in Korea ($L = 1000\text{km}$, 1100km , and 1200km). The horizontal axis gives the off-axis angle at SK and the vertical axis is that at the far detector locations. The purple line shows the off-axis angle at Oki Island. The red, blue, and black lines are the smallest off-axis angle at $L = 1000\text{km}$, 1100km and 1200km , respectively. The points corresponding to the purple circles and black squares are used in our numerical analysis.

3.2 Off-axis angles and beam profiles

Figure 3 shows the relation among the off-axis angles of the neutrino beam from J-PARC observable at SK, Oki, and a far detector in Korea ($L = 1000\text{km}$, 1100km , and 1200km). The horizontal axis gives the off-axis angle at SK and the vertical axis gives the corresponding off-axis angles at far detector locations. The purple line shows the off-axis angle at Oki Island, which grows as that at SK is increased, because both SK and Oki Island is located in the east (upper) side of the beam center of the T2K neutrino beam; see Fig. 1. The red, blue, and black lines are the smallest off-axis angle observable in Korea at $L = 1000\text{km}$, 1100km , and 1200km , respectively. In contrast to the Oki Island case, the off-axis angle at Korea decreases as that at SK grows, because Korea is in the west (lower) side of the beam center, also as shown in Fig. 1. The points corresponding to the purple circles and black squares in the figure are used in our numerical analysis in the following sections.

In Fig. 4, the beam profiles of the three off-axis beams (OAB) with 2.0° , 2.5° , and 3.0° off-axis angles at SK are shown at SK, Oki Island (three purple circles in Fig. 3) and at $L = 1000\text{km}$ in Korea (three black squares in Fig. 3), together with the $\nu_\mu \rightarrow \nu_e$ and $\bar{\nu}_\mu \rightarrow \bar{\nu}_e$ oscillation probabilities as functions of the neutrino energy, E_ν in units of GeV. The left column panels are for the ν_μ focusing beam and the right column ones are for the $\bar{\nu}_\mu$ focusing beam. The upper three rows, (a1)-(a3) and (b1)-(b3), display the beam flux for the ν_μ and $\bar{\nu}_\mu$ focusing beam, respectively, at $L = 1 \text{ km}$ in units of $10^{10}/\text{cm}^2/10^{21}\text{POT}$ (protons on target). The first row, (a1) and (b1), gives the beam profile observable at each far detector for the 2.0° off-axis beam (OAB) at the SK (red solid line), which gives the

0.6° OAB at Oki Island (green dashed line), and the 1.5° OAB for a far detector in Korea at $L = 1000$ km (blue dotted line). The second row, (a2) and (b2), is for the 2.5° OAB at SK, which gives the 0.9° OAB at Oki Island, and the 1.0° OAB at $L = 1000$ km. The case for the 3.0° OAB at SK, which gives the 1.4° OAB at Oki Island and the 0.5° OAB at $L = 1000$ km, is shown in the third row. It is clearly seen that all fluxes at Oki and Korea are harder than those at SK. The hardest flux with $E^{\text{peak}} \gtrsim 1$ GeV is found for the 2.0° at SK beam at Oki, and for the 3.0° at SK beam in Korea. The 2.5° at SK beam gives almost the same flux shape of $\sim 1.0^\circ$ OAB at Oki and at the $L = 1000$ km location in Korea, as shown in Fig. 1. This may call upon the possibility of locating detectors both in Oki and in Korea, where both detectors observe exactly the same OAB around the off-axis angle of 1.0° .

The lower two rows in Fig. 4 show the $\nu_\mu \rightarrow \nu_e$ ($\bar{\nu}_\mu \rightarrow \bar{\nu}_e$) oscillation probability in the left (right) column, for the normal hierarchy, (P1) and (P3), and for the inverted hierarchy, (P2) and (P4). The oscillation probabilities are calculated for the average matter densities of eq. (28), and the three-neutrino-model parameters:

$$\delta m_{12}^2 = 7.5 \times 10^{-5} \text{ eV}^2, \quad (29a)$$

$$\delta m_{13}^2 = \pm 2.35 \times 10^{-3} \text{ eV}^2, \quad (29b)$$

$$\sin^2 \theta_{\text{ATM}} = 0.5, \quad (29c)$$

$$\sin^2 2\theta_{\text{SOL}} = 0.852, \quad (29d)$$

with

$$\sin^2 2\theta_{\text{RCT}} = 0.08, \quad (30a)$$

$$\delta_{\text{MNS}} = 0.0^\circ. \quad (30b)$$

The plus (minus) sign in eq. (29b) is taken for the normal (inverted) hierarchy, whose predictions are shown in the fourth (bottom) row of Fig. 4. The red solid line in these panels is the oscillation probability at the SK, the green dashed line is for Oki Island, and the blue dotted line is for a far detector in Korea, at $L = 1000$ km.

From the four plots (P1)~(P4) in the bottom two rows in Fig. 4, we find that the first oscillation peak at SK appears at E_ν around $0.4 \sim 0.6$ GeV for all the four cases, ν_μ vs $\bar{\nu}_\mu$ and for both hierarchies. Since the OAB peaks at around $E_\nu = 0.7, 0.6,$ and 0.5 GeV for $2.0^\circ, 2.5^\circ,$ and 3.0° , respectively, as shown by the red solid curves in the first three rows of Fig. 4, all the OAB at SK between 2.0° and 3.0° can observe $\nu_\mu \rightarrow \nu_e$ and $\bar{\nu}_\mu \rightarrow \bar{\nu}_e$ oscillations with good efficiency. On the other hand, the oscillation probabilities at Oki Island are high at E_ν around $1.0 \sim 1.4$ GeV from the green dashed curves in the bottom two rows, where the flux is slightly small for the 3.0° OAB at SK, as shown also by green dashed curves in the third row. Finally, at $L = 1000$ km, the $\nu_\mu \rightarrow \nu_e$ and $\bar{\nu}_\mu \rightarrow \bar{\nu}_e$ oscillation probabilities are large at around $E_\nu \sim 2$ GeV, and hence the OAB with 3.0° at SK is most favorable [26]-[29]. We will confirm the above observations for the whole region of the three neutrino model parameter space in the following sections.

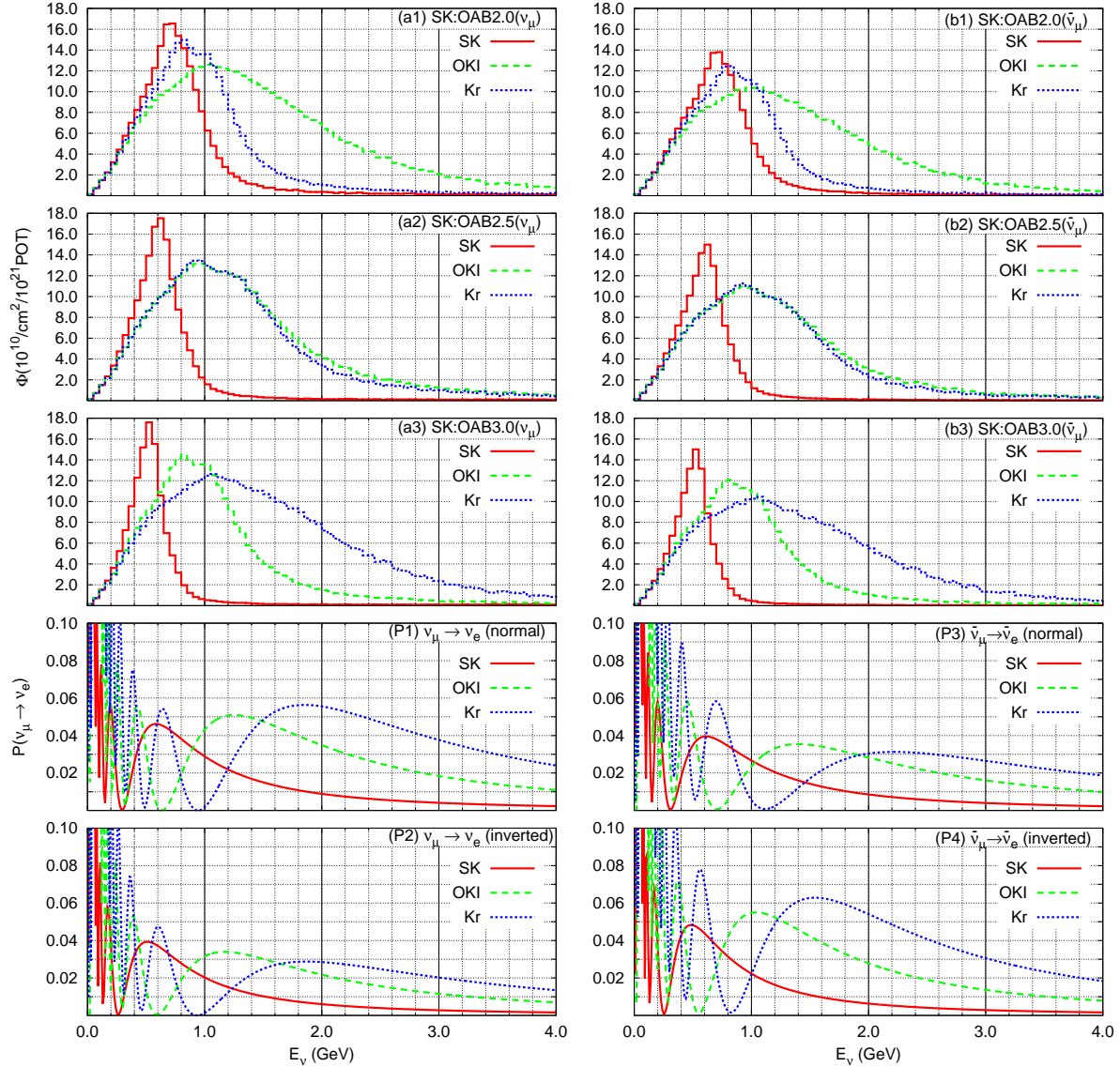


Figure 4: The beam profiles and the oscillation probabilities as functions of the neutrino energy. The left column panels are for the ν_μ focusing beam and the right ones are for the $\bar{\nu}_\mu$ focusing beam. The upper 6 panels, (a1)-(a3) and (b1)-(b3), show the beam fluxes at $L = 1$ km and the bottom 4 panels, (P1)-(P4), show the $\nu_\mu \rightarrow \nu_e$ ($\bar{\nu}_\mu \rightarrow \bar{\nu}_e$) oscillation probability with the input parameters of eqs. (28) and (29) for $\sin^2 2\theta_{\text{RCT}} = 0.08$ and $\delta_{\text{MNS}} = 0^\circ$. The first row, (a1) and (b1) gives the beam profile at each far detector for the 2.0° off-axis beam (OAB) at SK, the second row, (a2) and (b2) is for the 2.5° OAB at SK, and the third row, (a3) and (b3) is for the 3.0° OAB at SK. The fourth row, (P1) and (P3), shows the $\nu_\mu \rightarrow \nu_e$ and $\bar{\nu}_\mu \rightarrow \bar{\nu}_e$ oscillation probability for the normal hierarchy, respectively, and the bottom row, (P2) and (P4), is for the inverted hierarchy.

4 Typical event numbers at each detector

In this section, we explain how we estimate event numbers at each far detector.

4.1 Event calculation

In order to compare the physics capability of the T2KO experiment and that of T2KK experiment with a far detector at various baseline lengths and OAB's, we adopt the same conditions as those in Refs. [26, 27, 30]: All the detectors at Kamioka, Oki Island, and Korea are assumed to have excellent detection and kinematical reconstruction capabilities for ν_μ and ν_e Charged Current Quasi-Elastic (CCQE) events within the fiducial volumes of the 22.5 kton at Kamioka (SK) and 100 kton at Oki Island or in Korea. We use the neutrino fluxes of J-PARC beam at various off-axis angles [43] and the CCQE cross sections off water target [45] to compute event numbers as functions of (reconstructed) neutrino energy with the bin width of $\delta E_\nu = 200$ MeV at $E_\nu > 400$ MeV. The energy bin width of 200 MeV is chosen to take account of kinematical reconstruction errors due to Fermi motion, resonance production and detector resolutions [29]. We take account of background from secondary beams, such as ν_e , $\bar{\nu}_e$ and $\bar{\nu}_\mu$ fluxes for the ν_μ focusing beam, but we do not consider other backgrounds including the single π^0 production from the neutral current (NC) events [29]. In other words, the results of our studies show what a perfect detector of a given fiducial volume can achieve with neutrino beams from J-PARC when it is placed along the T2K beam line. Reconstruction efficiency and errors as well as the background rejection capabilities depend on specific detector designs and their studies are beyond the scope of this paper.

The number of ν_α CCQE events from the ν_β flux in the ν_μ -focusing beam in the n -th energy bin, $E_\nu^n = E_\nu^{\text{th}} + (n - 1) \times \delta E_\nu < E_\nu < E_\nu^n + \delta E_\nu$, at each site are calculated as

$$N_{\text{D}}^n(\nu_\beta \rightarrow \nu_\alpha) = M_{\text{D}} N_{\text{A}} \int_{E_\nu^n}^{E_\nu^n + \delta E_\nu} \Phi_{\nu_\beta}(E) P_{\nu_\beta \rightarrow \nu_\alpha}(E) \sigma_\alpha^{\text{CCQE}}(E) dE, \quad (31)$$

where the suffix ‘‘D’’ denotes the place of the far detector (D=SK, Oki, Kr), $\nu_{\alpha,\beta}$ is neutrino or anti-neutrino flavor ($\nu_{\alpha,\beta} = \nu_\mu, \nu_e, \bar{\nu}_\mu, \bar{\nu}_e$), M_{D} is the fiducial mass of each detector ($M_{\text{SK}} = 22.5$ kton and $M_{\text{Oki}} = M_{\text{Kr}} = 100$ kton), $N_{\text{A}} = 6.017 \times 10^{23}$ is the Avogadro number, Φ_{ν_β} is the ν_β flux from J-PARC [43] which scales as $1/L^2$, $P_{\nu_\beta \rightarrow \nu_\alpha}$ is the neutrino or anti-neutrino oscillation probability calculated by eq. (15) with the average matter density of eq. (28), and $\sigma_\alpha^{\text{CCQE}}$ is the CCQE cross sections per nucleon in water for each flavor type [45]. We also define the event number for $\bar{\nu}_\mu$ focusing beam as

$$\bar{N}_{\text{D}}^n(\nu_\beta \rightarrow \nu_\alpha) = M_{\text{D}} N_{\text{A}} \int_{E_\nu^n}^{E_\nu^n + \delta E_\nu} \bar{\Phi}_{\nu_\beta}(E) P_{\nu_\beta \rightarrow \nu_\alpha}(E) \sigma_\alpha^{\text{CCQE}}(E) dE, \quad (32)$$

where $\bar{\Phi}_{\nu_\beta}$ gives the ν_β flux in the $\bar{\nu}_\mu$ focusing beam [43].

Because we only consider the contribution from the secondary neutrino fluxes of the primary beam as the background in this analysis, each e - and μ -like event numbers in the n -th bin are calculated as

$$N_{\alpha,\text{D}}^n = \sum_{\beta=e,\mu} \{N_{\text{D}}^n(\nu_\beta \rightarrow \nu_\alpha) + N_{\text{D}}^n(\bar{\nu}_\beta \rightarrow \bar{\nu}_\alpha)\}, \quad (33)$$

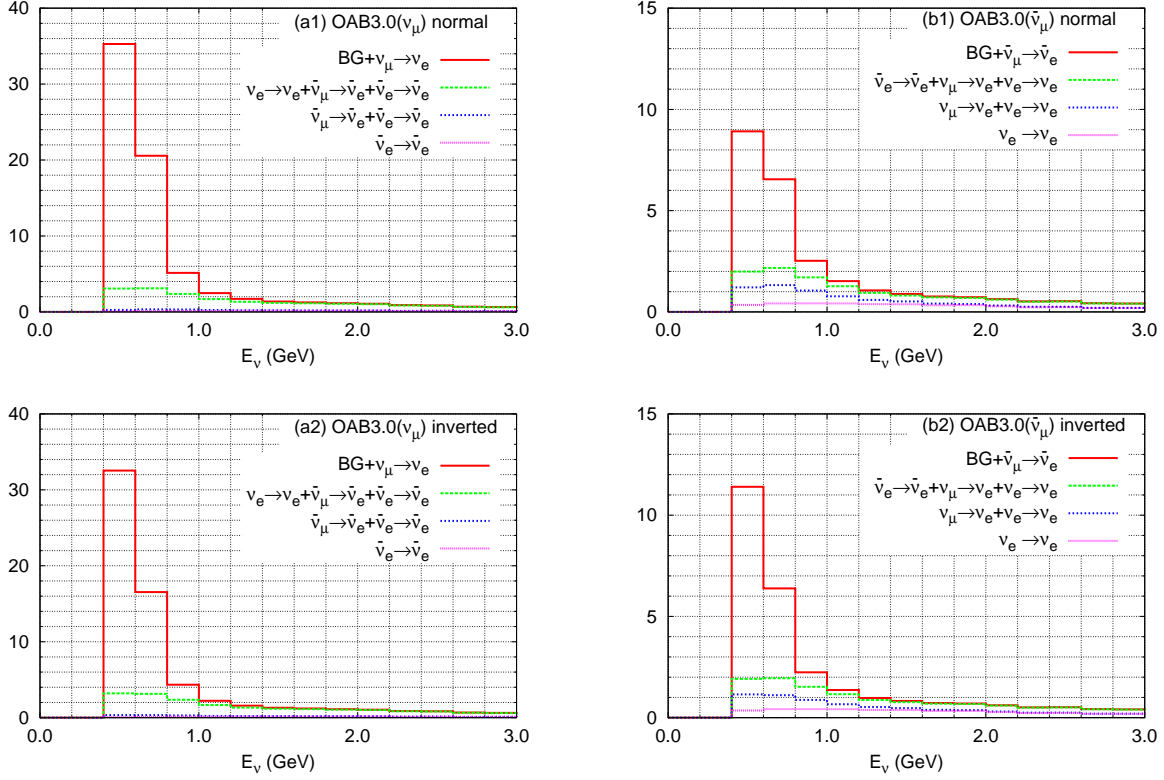


Figure 5: Typical event number of the e -like CCQE events for E_ν ($E_{\bar{\nu}}$) > 0.4 GeV at SK (22.5kton) with 3.0° off-axis angle and 2.5×10^{21} POT exposure: (a1) and (a2) are for ν_μ focusing beam, and (b1) and (b2) are for $\bar{\nu}_\mu$ focusing beam; whereas (a1) and (b1) are for the normal hierarchy, and (a2) and (b2) are for the inverted hierarchy. The results are for $\sin^2 2\theta_{\text{RCT}} = 0.08$, $\delta_{\text{MNS}} = 0^\circ$, and $\bar{\rho}_{\text{T2K}} = 2.60$ g/cm 3 and the other input parameters of eq. (29). The red solid line in each panel denotes the total event numbers, the purple dotted line shows the $\bar{\nu}_e \rightarrow \bar{\nu}_e$ contribution in (a1) and (a2), $\nu_e \rightarrow \nu_e$ in (b1) and (b2), the blue short dashed line gives the sum of the contributions from $\bar{\nu}_\mu \rightarrow \bar{\nu}_e$ and $\bar{\nu}_e \rightarrow \bar{\nu}_e$ in (a1) and (a2), that of $\nu_\mu \rightarrow \nu_e$ and $\nu_e \rightarrow \nu_e$ in (b1) and (b2), and the green dashed line shows the total background contribution from the secondary beams.

for $\alpha = e, \mu$ at each far detector “D” (D=SK, Oki, Kr). We also define the event numbers with $\bar{\nu}_\mu$ focusing beam as

$$\bar{N}_{\alpha, \text{D}}^n = \sum_{\beta=e, \mu} \{ \bar{N}_{\text{D}}^n(\bar{\nu}_\beta \rightarrow \bar{\nu}_\alpha) + \bar{N}_{\text{D}}^n(\nu_\beta \rightarrow \nu_\alpha) \}, \quad (34)$$

for $\alpha = e, \mu$ at each far detector.

4.2 SK

The typical event numbers of the e -like CCQE events for E_ν ($E_{\bar{\nu}}$) > 0.4 GeV at SK (22.5 kton) with the 3.0° OAB and 2.5×10^{21} POT exposure is shown in Fig. 5: (a1) and (a2) are for the ν_μ focusing, and (b1) and (b2) are for the $\bar{\nu}_\mu$ focusing beam; (a1) and

(b1) are for the normal, and (a2) and (b2) are for the inverted hierarchy. These results are for $\sin^2 2\theta_{\text{RCT}} = 0.08$, $\delta_{\text{MNS}} = 0^\circ$ and $\bar{\rho}_{\text{T2K}} = 2.60\text{g/cm}^3$ the other input parameters of eq. (29). In each panel, the red solid line denotes the total event number, which is the sum of the signal events, $\nu_\mu \rightarrow \nu_e$ for (a1) and (a2), or $\bar{\nu}_\mu \rightarrow \bar{\nu}_e$ for (b1) and (b2), and the total background from the secondary beams shown by the green dashed line. The purple dotted line shows the $\bar{\nu}_e \rightarrow \bar{\nu}_e$ contribution in (a1) and (a2), $\nu_e \rightarrow \nu_e$ in (b1) and (b2). The blue short dashed line gives the sum of the contributions from $\bar{\nu}_\mu \rightarrow \bar{\nu}_e$ and $\bar{\nu}_e \rightarrow \bar{\nu}_e$ in (a1) and (a2), and those from $\nu_\mu \rightarrow \nu_e$ and $\nu_e \rightarrow \nu_e$ in (b1) and (b2).

In Fig. 5, both the signal (red solid minus green dash) and the total (red solid) number of events peak in the first bin ($400 \text{ MeV} < E_\nu < 600 \text{ MeV}$), because both the 3.0° OAB fluxes and the oscillation probabilities are largest in the region; see Fig. 4, (a3), (P1), and (P2) for $\nu_\mu \rightarrow \nu_e$, (b3), (P3), and (P4) for $\bar{\nu}_\mu \rightarrow \bar{\nu}_e$. The background levels are higher for the $\bar{\nu}_\mu \rightarrow \bar{\nu}_e$ oscillation experiments than the $\nu_\mu \rightarrow \nu_e$ case for both hierarchies. This is partly because of the higher level of the secondary beam fluxes in the $\bar{\nu}_\mu$ focusing beam [43], and partly because the CCQE cross sections are larger for ν_ℓ than the $\bar{\nu}_\ell$ ($\ell = \mu, e$) [45].

Since the ratio of the $\bar{\nu}_\mu \rightarrow \bar{\nu}_e$ to the $\nu_\mu \rightarrow \nu_e$ event numbers is significantly larger for the inverted hierarchy than that for the normal hierarchy case in Fig. 5, one may be tempted to conclude that the neutrino mass hierarchy can be determined by using both ν_μ and $\bar{\nu}_\mu$ focusing beams at T2K. This is not the case since the same trend can be expected for $\sin \delta_{\text{MNS}} \sim -1$, as can be seen clearly from eq. (27a).

4.3 Oki Island

Figure 6 shows the typical event numbers for the e -like CCQE event at Oki Island ($L = 653 \text{ km}$), where we suppose to place a 100 kton fiducial volume detector. The results are for 2.5×10^{21} POT at J-PARC for both ν_μ and $\bar{\nu}_\mu$ focusing beam at the off-axis angle of 1.4° , which corresponds to the 3.0° OAB at SK, as shown in Fig. 3. We use eqs. (29) and (30) for physics parameters and eq. (28b) for the average matter density to generate these event numbers. The left two panels in Fig. 6, (a1) and (a2), are for the ν_μ focusing beam, while the right two panels (b1) and (b2) are for the $\bar{\nu}_\mu$ focusing beam. The top two panels, (a1) and (b1), are for the normal mass hierarchy, and the bottom two panels, (a2) and (b2), are for the inverted mass hierarchy. The line types are the same as in Fig. 5, the red solid lines give the total event numbers, the green dashed lines are the sum of all the background events from secondary beams, the blue short dashed lines give the sum of $\bar{\nu}_\mu \rightarrow \bar{\nu}_e$ and $\bar{\nu}_e \rightarrow \bar{\nu}_e$ for the ν_μ focusing beam, that of $\nu_\mu \rightarrow \nu_e$ and $\nu_e \rightarrow \nu_e$ for the $\bar{\nu}_\mu$ focusing beam. The purple dotted lines shows the contribution from $\nu_e \rightarrow \nu_e$ ($\bar{\nu}_e \rightarrow \bar{\nu}_e$) for ν_μ ($\bar{\nu}_\mu$) focusing beam. As in the case of SK shown in Fig. 5, the background from the secondary beam contributions are higher for the $\bar{\nu}_\mu$ focusing beam than those for the ν_μ focusing beam.

In Fig. 6, we find that the first oscillation peak appears at around 1.0 GeV at Oki Island

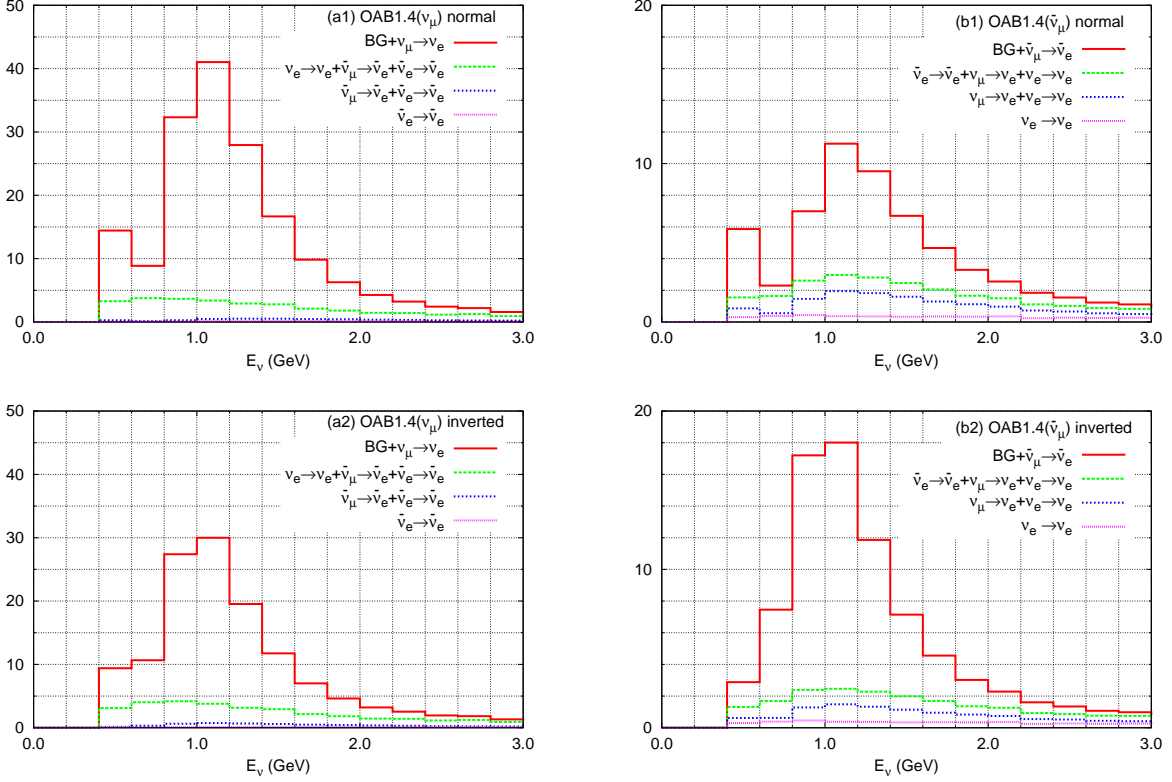


Figure 6: The same as Fig. 5, but for Tokai-to-Oki Island ($L = 653\text{km}$), where the fiducial volume of 100 kton and the off-axis angle of 1.4° is assumed for the far detector. The results are for $\sin^2 2\theta_{\text{RCT}} = 0.08$ and $\delta_{\text{MNS}} = 0^\circ$, and $\bar{\rho}_{\text{T2OKI}} = 2.75 \text{ g/cm}^3$, see eq. (28b).

for all the four cases. The peaks at $E_\nu \sim 1 \text{ GeV}$ in the event numbers are obtained by the convolution of the oscillation probability, whose first peak is located around $E_\nu \sim 1.2 \text{ GeV}$ for the normal or slightly above 1 GeV for the inverted hierarchy, as shown in Fig. 4 (P1)-(P4), and the 1.4° OAB fluxes that have a peak at around 0.8 GeV in Fig. 4 (a3) and (b3), as shown by green dashed lines. The difference between the normal and inverted hierarchy is larger than that of the T2K experiment. One can observe the second peak in the $400\sim 600 \text{ MeV}$ bin for the normal hierarchy case, (a1) and (b1), but not for the inverted case. This is because the matter effect to the oscillation phase, the term B^e in eqs. (22) and (23b), grows with the baseline length L , and shifts the peaks of the oscillation maximum at $|\Delta_{13} + B^e| \sim \pi, 3\pi, \dots$ in the opposite directions; toward higher (lower) energies for the normal (inverted) hierarchy. More accurately speaking, the above phase shift pattern applies for $\cos \delta_{\text{MNS}} \sim 1$, as can be read off from eq. (23b), where the matter effect diminishes (enhances) the shift for the normal (inverted) hierarchy. The pattern reverses for $\cos \delta_{\text{MNS}} \sim -1$. Likewise, the matter effects on the oscillation amplitudes are also clearly seen: we expect more (less) $\nu_\mu \rightarrow \nu_e$ events than $\bar{\nu}_\mu \rightarrow \bar{\nu}_e$ events around the first oscillation peak when the hierarchy is normal (inverted) as can be seen from eq. (23a). This pattern is enhanced when $\sin \delta_{\text{MNS}} \sim -1$ whereas it is diminished when $\sin \delta_{\text{MNS}} \sim 1$.

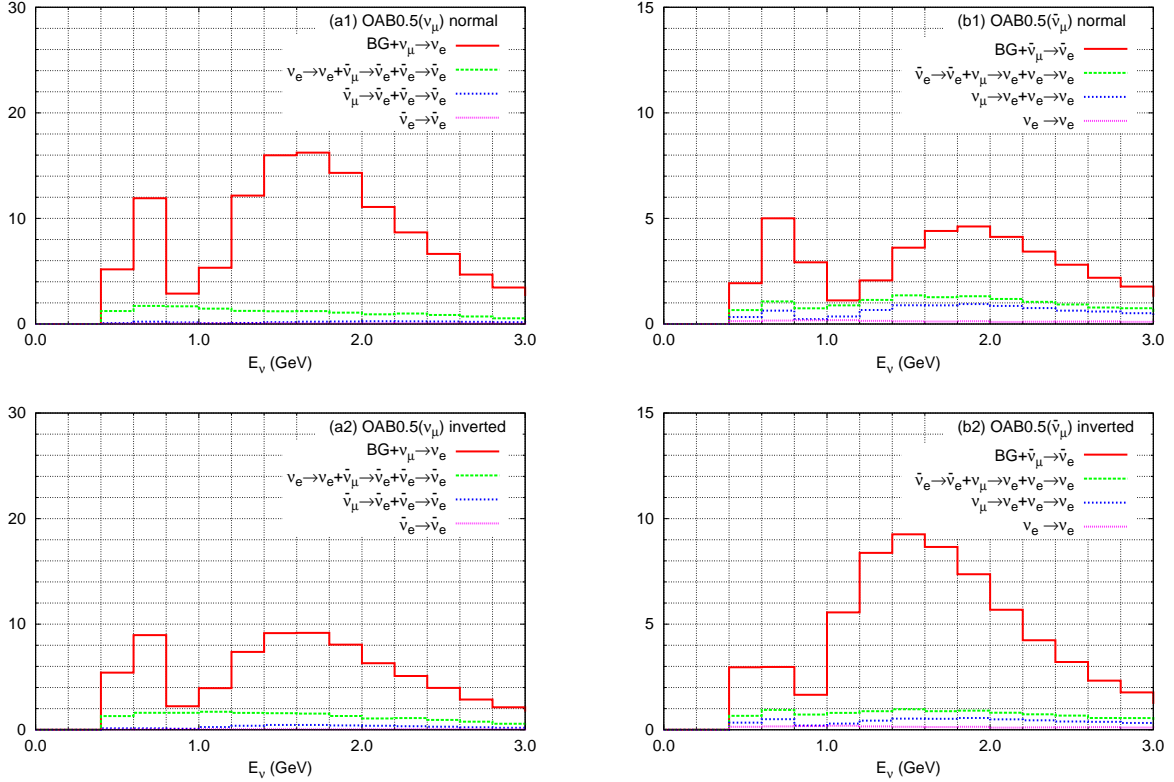


Figure 7: The same as Fig. 5, but for Korea ($L = 1000\text{km}$), where the fiducial volume of 100 kton and the off-axis angle of 0.5° is assumed for the far detector. The results are for $\sin^2 2\theta_{\text{RCT}} = 0.08$ and $\delta_{\text{MNS}} = 0^\circ$, and $\bar{\rho}_{\text{T2OKi}} = 2.9 \text{ g/cm}^3$, see eq. (28c).

4.4 Korea

In Figs. 7, we show the typical event numbers for e -like CCQE event at a far detector in Korea ($L = 1000 \text{ km}$) with a 100 kton fiducial volume detector. The off-axis angle there is chosen to be 0.5° , which optimized the T2KK performance with the 3.0° OAB at SK [26, 27, 29]. The results are for $\sin^2 2\theta_{\text{RCT}} = 0.8$ and $\delta_{\text{MNS}} = 0^\circ$ and the parameters of eqs. (29) and (30), with the average matter density of 2.9 g/cm^3 eq. (28c). The panels and the lines types are the same as those in Figs. 5 and 6.

The first peak of the event appears at around 1.6 GeV for the ν_μ beam for both hierarchies, but that is around 1.8 (1.5) GeV for the $\bar{\nu}_\mu$ beam for the normal (inverted) hierarchy. This is because of the matter effect contribution to the oscillation phase, B^e in eq. (23b), and \bar{B}^e obtained from eq. (23b) by reversing the sign of $\bar{\rho}$. The magnitude of B^e is small for $\cos \delta_{\text{MNS}} = 1$ in eq. (23b), whereas that of \bar{B}^e is enhanced. As expected, the sign of the difference $B^e - \bar{B}^e$ in eq. (27b) reflects the neutrino mass hierarchy.

Likewise, the difference in the heights of the first oscillation peak is more distinct in Fig. 7 for $L = 1000 \text{ km}$ than that in Fig. 6 for $L = 653 \text{ km}$. As expected, the oscillation amplitude for the $\nu_\mu \rightarrow \nu_e$ transition is bigger (smaller) than that for the $\bar{\nu}_\mu \rightarrow \bar{\nu}_e$ transition when the hierarchy is normal (inverted). Although the magnitudes of those enhancement or suppression factor depends on $\sin \delta_{\text{MNS}}$, as can be seen from eqs. (23a) and (27a), the

difference between different baseline lengths among Figs. 5, 6, and 7 depend solely on the mass hierarchy pattern, as expressed in eq. (24).

5 Analysis method

We introduce a $\Delta\chi^2$ function

$$\Delta\chi^2 \equiv \chi_{\text{stat}}^2 + \chi_{\text{sys}}^2 + \chi_{\text{para}}^2, \quad (35)$$

in order to compare the physics potential of T2K, T2KO, and T2KK experiments quantitatively on the same footing. The first term of eq. (35) gives statistical constraints on the model parameters from the number of the CCQE events in each bin at each detector:

$$\chi_{\text{stat}}^2 = \sum_{\text{D}} \sum_n \left\{ \left(\frac{(N_{\mu,\text{D}}^n)^{\text{input}} - (N_{\mu,\text{D}}^n)^{\text{fit}}}{\sqrt{(N_{\mu,\text{D}}^n)^{\text{input}}}} \right)^2 + \left(\frac{(N_{e,\text{D}}^n)^{\text{input}} - (N_{e,\text{D}}^n)^{\text{fit}}}{\sqrt{(N_{e,\text{D}}^n)^{\text{input}}}} \right)^2 + \left(\frac{(\bar{N}_{\mu,\text{D}}^n)^{\text{input}} - (\bar{N}_{\mu,\text{D}}^n)^{\text{fit}}}{\sqrt{(\bar{N}_{\mu,\text{D}}^n)^{\text{input}}}} \right)^2 + \left(\frac{(\bar{N}_{e,\text{D}}^n)^{\text{input}} - (\bar{N}_{e,\text{D}}^n)^{\text{fit}}}{\sqrt{(\bar{N}_{e,\text{D}}^n)^{\text{input}}}} \right)^2 \right\}, \quad (36)$$

where $N_{\mu,\text{D}}^n$ and $N_{e,\text{D}}^n$ denotes the number of μ - and e -like events, respectively, for the ν_μ focusing beam calculated with eq. (33) in the n -th bin at each detector, D=SK, Oki, Kr, whereas $\bar{N}_{\mu,\text{D}}^n$ and $\bar{N}_{e,\text{D}}^n$ are for the $\bar{\nu}_\mu$ focusing beam. Their square-roots give statistical errors. The summation is over all bins from 0.4 GeV to 5.0 GeV for μ -like events at all sites, and for e -like events from 0.4 GeV to 1.2 GeV at SK, from 0.4 GeV to 2.4 GeV at Oki, from 0.4 GeV to 2.8 GeV at a far detector in Korea, respectively. The input event numbers, $(N_{\alpha,\text{D}}^n)^{\text{input}}$, are generated with eq. (29) for both hierarchies, and for various value of $\sin^2 2\theta_{\text{RCT}}$ and δ_{MNS} . We use the average matter density along each baseline of eq. (28) when we calculate the input event numbers.

The event numbers in the fit, $(N_{\alpha,\text{D}}^n)^{\text{fit}}$ and $(\bar{N}_{\alpha,\text{D}}^n)^{\text{fit}}$, are obtained by varying all the 6 parameters of the three-neutrino model freely and also by allowing for the systematic errors. We consider the following systematic errors in this analysis. We assign 6% uncertainty to the overall matter density along each baseline,

$$\bar{\rho}_{\text{D}}^{\text{fit}} = f_{\rho}^{\text{D}} \bar{\rho}_{\text{D}}, \quad f_{\rho}^{\text{D}} = 1.00 \pm 0.06, \quad (\text{for D=SK, Oki, Kr}). \quad (37)$$

Although we expect positive correlation among f_{ρ}^{D} , we allow them to vary independently as a conservative estimate. We assign 3% uncertainty in the flux normalization of ν_μ and $\bar{\nu}_\mu$ focusing beam as

$$(\Phi_{\nu_\alpha}^{\text{D}})^{\text{fit}} = f_{\nu_\alpha}^{\text{D}} \Phi_{\nu_\alpha}^{\text{D}}, \quad f_{\nu_\alpha}^{\text{D}} = 1.00 \pm 0.03, \quad (\text{for } \nu_\alpha = \nu_\mu, \nu_e, \bar{\nu}_\mu, \nu_e), \quad (38a)$$

$$(\bar{\Phi}_{\nu_\alpha}^{\text{D}})^{\text{fit}} = \bar{f}_{\nu_\alpha}^{\text{D}} \bar{\Phi}_{\nu_\alpha}^{\text{D}}, \quad \bar{f}_{\nu_\alpha}^{\text{D}} = 1.00 \pm 0.03, \quad (\text{for } \nu_\alpha = \nu_\mu, \nu_e, \bar{\nu}_\mu, \nu_e), \quad (38b)$$

respectively, where D=SK, Oki, Kr. We also ignore possible correlations among the flux errors. For the CCQE cross sections of neutrino and anti-neutrinos, we assume common

3% error as

$$\left(\sigma_{\nu_{\mu,e}}^{\text{CCQE}}(E)\right)^{\text{fit}} = f_{\ell} \left(\sigma_{\nu_{\mu,e}}^{\text{CCQE}}(E)\right), \quad f_{\ell} = 1.00 \pm 0.03, \quad (39a)$$

$$\left(\sigma_{\bar{\nu}_{\mu,e}}^{\text{CCQE}}(E)\right)^{\text{fit}} = f_{\bar{\ell}} \left(\sigma_{\bar{\nu}_{\mu,e}}^{\text{CCQE}}(E)\right), \quad f_{\bar{\ell}} = 1.00 \pm 0.03, \quad (39b)$$

for neutrino and anti-neutrino events, independently, but we take $f_{\nu_{\mu}} = f_{\nu_e} = f_{\ell}$ and $f_{\bar{\nu}_{\mu}} = f_{\bar{\nu}_e} = f_{\bar{\ell}}$ because of the $e\text{-}\mu$ universality. Here also, we neglect the correlation between ν_{ℓ} and $\bar{\nu}_{\ell}$ cross section errors. The systematic error for the fiducial volume of each far detector is also assigned as

$$M_{\text{D}}^{\text{fit}} = f_{\text{D}} M_{\text{D}}, \quad f_{\text{D}} = 1.00 \pm 0.03 \quad (\text{for D} = \text{SK, Oki, Kr}). \quad (40)$$

Summing up, we take account of 32 systematic uncertainties in terms of which χ_{sys}^2 in eq. (35) is expressed as

$$\begin{aligned} \chi_{\text{sys}}^2 = & \sum_{\text{D}} \left[\left(\frac{1-f_{\text{D}}}{0.03} \right)^2 + \left(\frac{1-f_{\rho}^{\text{D}}}{0.06} \right)^2 + \sum_{\nu_{\alpha}} \left\{ \left(\frac{1-f_{\nu_{\alpha}}^{\text{D}}}{0.03} \right)^2 + \left(\frac{1-f_{\bar{\nu}_{\alpha}}^{\text{D}}}{0.03} \right)^2 \right\} \right] \\ & + \sum_{\beta=\ell,\bar{\ell}} \left(\frac{1-f_{\beta}}{0.03} \right)^2. \end{aligned} \quad (41)$$

There are 32 normalization factors since for each detector ‘‘D’’ the fiducial volume (f_{D}), the average matter density (f_{ρ}^{D}), and the 4 fluxes each for ν_{μ} ($f_{\nu_{\alpha}}^{\text{D}}$) and $\bar{\nu}_{\mu}$ ($f_{\bar{\nu}_{\alpha}}^{\text{D}}$) focusing beam are accounted for, in addition to the overall theoretical uncertainties for ν_{ℓ} (f_{ℓ}) and $\bar{\nu}_{\ell}$ ($f_{\bar{\ell}}$) CCQE cross sections.

The last term of eq. (35), χ_{para}^2 , accounts for the external constraints on the model parameters:

$$\begin{aligned} \chi_{\text{para}}^2 = & \left(\frac{7.5 \times 10^{-5} \text{eV}^2 - (\delta m_{12}^2)^{\text{fit}}}{0.2 \times 10^{-5}} \right)^2 + \left(\frac{0.852 - \sin^2 2\theta_{\text{SOL}}^{\text{fit}}}{0.025} \right)^2 \\ & + \left(\frac{\sin^2 2\theta_{\text{RCT}}^{\text{input}} - \sin^2 2\theta_{\text{RCT}}^{\text{fit}}}{0.01} \right)^2. \end{aligned} \quad (42)$$

The first two terms are from the present constraints from the KamLAND experiment [9] listed in eq. (2). In the last term, we assume that the new reactor experiments [16, 17, 23] will measure $\sin^2 2\theta_{\text{RCT}}$ with an uncertainty of 0.01 in the near future. We do not impose the present constraints on $|\delta m_{13}^2|$ and $\sin^2 2\theta_{\text{ATM}}$ given in eq. (1), since the experiments studied in this report will measure them more accurately.

6 mass hierarchy

In this section, we show physics capability of the T2KO experiment to determine the mass hierarchy and compare it with that of the T2KK [26]-[30] and the T2K₁₂₂ experiment.

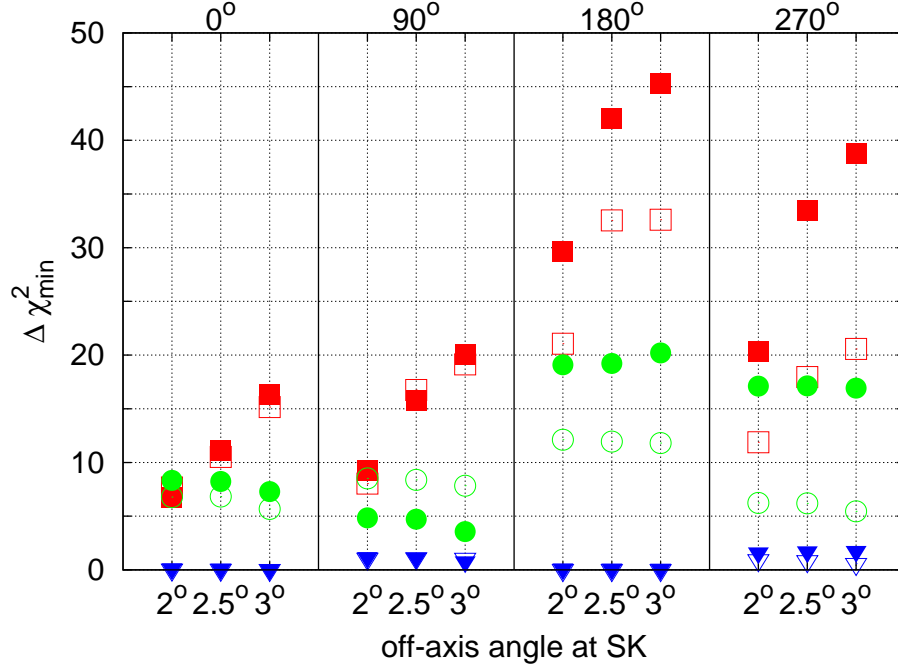


Figure 8: Minimum $\Delta\chi^2$ of the T2KK, T2KO, and T2K₁₂₂ experiment to exclude the wrong mass hierarchy when only the ν_μ focusing beam of 5.0×10^{21} POT is used. Four columns give results for $\delta_{\text{MNS}} = 0^\circ, 90^\circ, 180^\circ,$ and 270° , respectively, and the horizontal axis in each column gives the off-axis angle at SK. The solid (open) square, circle, and triangle denotes, respectively, the T2KK, T2KO and T2K₁₂₂ results for the normal (inverted) hierarchy. The results are for $\sin^2 2\theta_{\text{RCT}} = 0.08$ and the other input model parameters in eq. (29), as well as the average matter density of eq. (28) along the three baselines.

Here by T2K₁₂₂, we examine the option where the additional 100 kton detector is placed in the Kamioka site to make the total fiducial volume 122 kton at $L = 295$ km, which may be regarded as a small scale version of Hyper-Kamiokande [46].

In Fig. 8, we show the minimum $\Delta\chi^2$ of T2KK, T2KO, and T2K₁₂₂ experiment for the ν_μ focusing beam with 5.0×10^{21} POT. Four columns of Fig. 8 give results for $\delta_{\text{MNS}} = 0^\circ, 90^\circ, 180^\circ,$ and 270° , respectively, and the horizontal axis in each column gives the off-axis angle at the SK. The solid (open) square, circle, and triangle denotes, respectively, the sensitivity of the T2KK, T2KO, and T2K₁₂₂ experiments for the normal (inverted) hierarchy. The results are for $\sin^2 2\theta_{\text{RCT}} = 0.08$ and the other input model parameters in eq. (29), as well as the average matter density of eq. (28) along the three baselines.

From Fig. 8, we can tell that the physics potential for the mass hierarchy determination of the T2KK experiment is far better than the other experiments when the combination of 3.0° OAB at SK and 0.5° OAB at a far detector in Korea is taken, where the mass hierarchy can be determined by more than 4σ level for all the 8 cases (4 values of δ_{MNS} and both hierarchies). The sensitivity of the T2KK on the mass hierarchy reduces significantly as the off-axis angle at SK is reduced. This is because OAB with small off-axis angle cannot reach Korea when off-axis angle at SK is below $\sim 2.5^\circ$ [26, 27]; see Fig. 3.

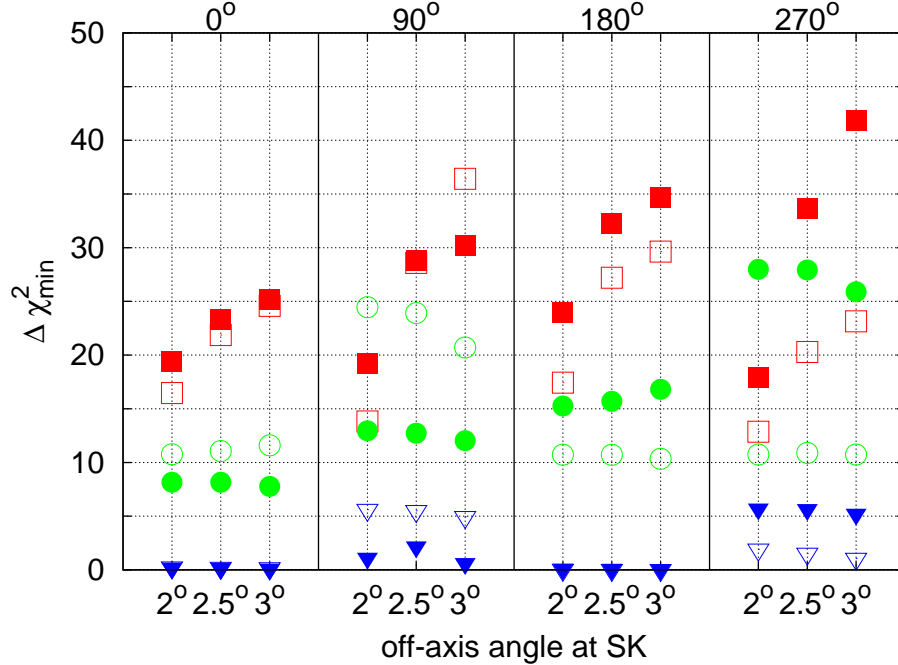


Figure 9: The same as Fig. 8, but with both ν_μ and $\bar{\nu}_\mu$ focusing beams each with 2.5×10^{21} POT.

For the T2KO experiment, the mass hierarchy can be determined at the 2σ level or higher. This capability does not depend strongly on the off-axis angle at SK, because the beam intensity around the first peak ($E_\nu \sim 1\text{GeV}$) at Oki Island does not change much with the OAB at SK, see Fig. 4.

Furthermore, it is clearly shown in Fig. 8 that the T2K₁₂₂ experiment does not have any sensitivity to the neutrino mass hierarchy pattern for any combinations of δ_{MNS} and the mass hierarchy. This is essentially because the small differences in the oscillation probabilities between the normal and the inverted hierarchy can easily be compensated by small shifts in the model parameters, such as $|\delta m_{13}^2|$, $\sin^2 \theta_{\text{ATM}}$, and δ_{MNS} .

In Fig. 9, we show the minimum $\Delta\chi^2$ of the T2KK, T2KO, and T2K₁₂₂ experiment to exclude the wrong mass hierarchy when both ν_μ and $\bar{\nu}_\mu$ focusing beams are used, each with 2.5×10^{21} POT to keep the total exposure the same.

As for the T2KK experiment, shown by the red squares, the improvement is significant especially when $\delta_{\text{MNS}} \simeq 0^\circ$ and 90° , making $\Delta\chi_{\text{min}}^2$ greater than 20 for all the 8 combinations of δ_{MNS} and $\text{sgn}(\delta m_{13}^2)$, not only for the 3.0° OAB but also for the 2.5° OAB at SK [30]. Likewise for the T2KO experiment, shown by green circles, the improvement is most significant at $\delta_{\text{MNS}} = 90^\circ$ where the smallest $\Delta\chi_{\text{min}}^2$ grows from ~ 4 in Fig. 8 to ~ 12 in Fig. 9. This is essentially because the $\sin \delta_{\text{MNS}}$ term in the oscillation amplitude shift A^e in eq. (23a) changes sign for the $\bar{\nu}_\mu \rightarrow \bar{\nu}_e$ oscillation as shown in eq. (27a) for the difference $A^e - \bar{A}^e$. This helps resolving the entanglement between the $\sin \delta_{\text{MNS}}$ dependence and the matter effect in the oscillation amplitudes. Significant improvements are also found for $\delta_{\text{MNS}} = 270^\circ$ by the same reason. Moderate improvements are found for the $\delta_{\text{MNS}} = 0^\circ$ case,

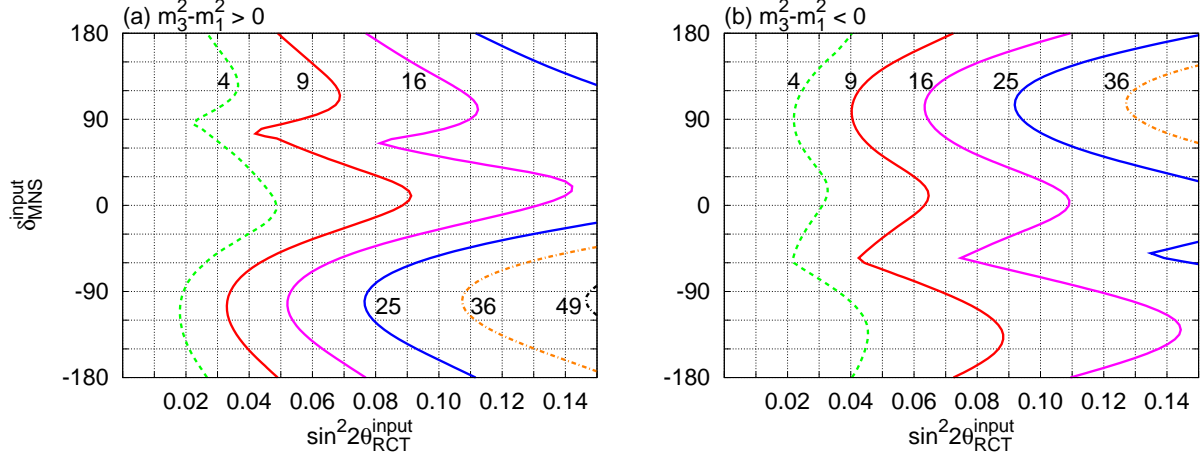


Figure 10: The $\Delta\chi_{\min}^2$ contour plot for the T2KO experiment to exclude the wrong mass hierarchy in the plane of $\sin^2 2\theta_{\text{RCT}}$ and δ_{MNS} . The left figure is for the normal hierarchy and the right one is for the inverted hierarchy. The OAB combination for both figures is 3.0° at SK and 1.4° at Oki Island with 2.5×10^{21} POT for both ν_μ and $\bar{\nu}_\mu$ focusing beams. Contours for $\Delta\chi_{\min}^2 = 4, 9, 16, 25, 36, 49$ are shown. All the input parameters other than $\sin^2 2\theta_{\text{RCT}}$ and δ_{MNS} are shown in eqs. (28) and (29).

allowing the T2KO experiment with half-and-half ν_μ and $\bar{\nu}_\mu$ beams to resolve the mass hierarchy at 3σ level for the worst case ($\delta_{\text{MNS}} = 0$ and normal hierarchy). No significant dependence on the OAB at SK is found.

The capability of determining the mass hierarchy pattern by the T2K₁₂₂ experiment does not appear even by using both ν_μ and $\bar{\nu}_\mu$ beams. The value of $\Delta\chi_{\min}^2$ stays almost zero, except for just two special combinations; $\delta_{\text{MNS}} = 270^\circ$ for the normal hierarchy and $\delta_{\text{MNS}} = 90^\circ$ for the inverted hierarchy. These are the two cases, where the difference between the $\nu_\mu \rightarrow \nu_e$ and $\bar{\nu}_\mu \rightarrow \bar{\nu}_e$ oscillation amplitudes, $A^e - \bar{A}^e$ in eq. (27a) is largest or smallest, respectively, such that variation of the other model parameters cannot account for the difference if the wrong mass hierarchy is assumed. With the same token, $\Delta\chi_{\min}^2$ exceeds 20 for T2KO or 30 for T2KK (with $\gtrsim 2.5^\circ$ OAB at SK) for these two particular combinations.

So far, we have shown results for $\sin^2 2\theta_{\text{RCT}} = 0.8$ and 4 representative values of δ_{MNS} ; $0^\circ, 180^\circ$, and $\pm 90^\circ$. In Fig. 10, we show the contour plot of the $\Delta\chi_{\min}^2$ for the T2KO experiment to exclude the wrong mass hierarchy in the whole plane of $\sin^2 2\theta_{\text{RCT}}$ and δ_{MNS} : The left figure (a) is for the normal hierarchy, whereas the right one (b) is for the inverted mass hierarchy. Since no strong dependence of $\Delta\chi_{\min}^2$ on the OAB angle is found for T2KO potential in Fig. 10, we choose 3.0° OAB at SK, which gives 1.4° OAB at Oki, as shown in Fig. 3. The results are for 2.5×10^{21} POT each for ν_μ and $\bar{\nu}_\mu$ focusing beam. Contours in each figure are for $\Delta\chi_{\min}^2 = 4, 9, 16, 25, 36$, and 49 . The input parameters other than $\sin^2 2\theta_{\text{RCT}}$ and δ_{MNS} are shown in eqs. (28) and (29), exactly the same as those adopted in Fig. 9. Accordingly the $\Delta\chi_{\min}^2$ values at $\sin^2 2\theta_{\text{RCT}} = 0.08$ agree exactly with those presented in Fig. 9 for T2KO with 3.0° OAB at SK, for the 4 representative δ_{MNS} values.

It is clearly seen from Fig. 10 that the mass hierarchy pattern can be distinguished at 3σ if $\sin^2 2\theta_{\text{RCT}}^{\text{input}} \gtrsim 0.09$ for any value of $\delta_{\text{MNS}}^{\text{input}}$ and for both hierarchies. The most difficult

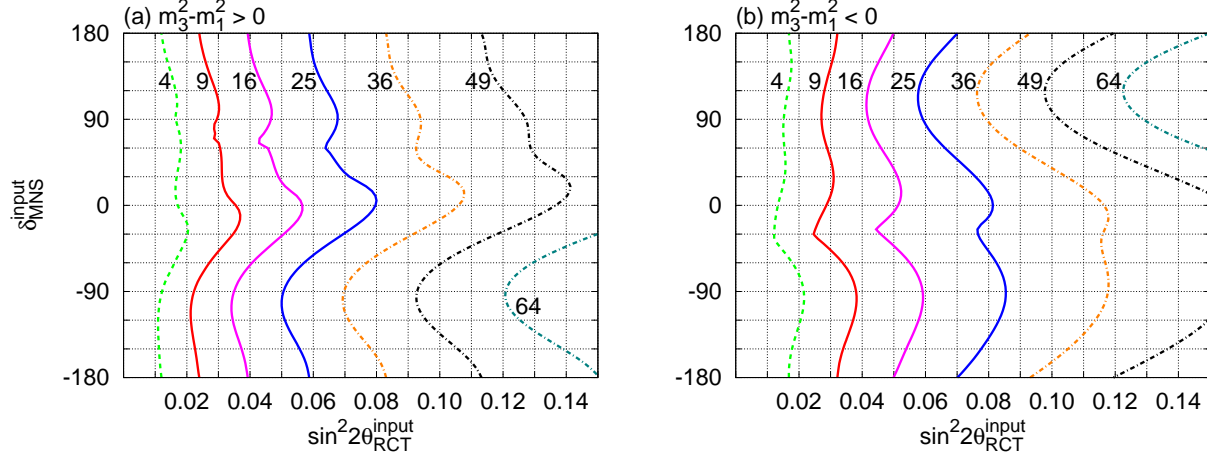


Figure 11: The same as Fig. 10, but for T2KK experiment with the optimum OAB combination, 3.0° OAB at SK and 0.5° OAB at $L = 1000\text{km}$. $\Delta\chi_{\min}^2$ values are given along the contours.

case is found for $\delta_{\text{MNS}} \sim 0^\circ$ for the normal hierarchy, while $\delta_{\text{MNS}} \sim -135^\circ$ for the inverted hierarchy. On the other hand, the discrimination is easiest at $\delta_{\text{MNS}} \sim -90^\circ$ for the normal and at $\delta_{\text{MNS}} \sim 90^\circ$ for the inverted hierarchy, in accordance with the argument presented above for Fig. 9.

In addition, the contour plots Fig. 10 identify another case at $\delta_{\text{MNS}} \simeq 60^\circ$ ($\simeq -60^\circ$) for the normal (inverted) hierarchy, where the difference between the right and the wrong hierarchy is large, giving high $\Delta\chi_{\min}^2$. The spikes of the contours around these δ_{MNS} values appear as a consequence of the conspiracy between the mass hierarchy dependences in the oscillation amplitude A^e and in the phase shift term B^e . When $\delta_{\text{MNS}}^{\text{input}} \simeq 60^\circ$, the $\nu_\mu \rightarrow \nu_e$ oscillation amplitude shift A^e cancels between the matter effect term and the $\sin \delta_{\text{MNS}}$ term for the normal (inverted) hierarchy at around the Tokai-to-Oki baseline; see eq. (23a) at $L = 653\text{ km}$. The cancellation is not significant at $L = 295\text{ km}$ for T2K, and the two effects add up constructively for $\bar{\nu}_\mu \rightarrow \bar{\nu}_e$ oscillation. When the wrong hierarchy is assumed the best fit is found for $\sin \delta_{\text{MNS}}^{\text{fit}} \sim 0$, for which there are two solutions, $\cos \delta_{\text{MNS}}^{\text{fit}} \sim 1$ and $\cos \delta_{\text{MNS}}^{\text{fit}} \sim -1$, which have significantly different phase-shift; see eq. (23b). We find that the spike around $\delta_{\text{MNS}} \sim \pm 60^\circ$ in Fig. 10 occurs when the $\Delta\chi_{\min}^2$ solution of the wrong hierarchy model jumps from $\cos \delta_{\text{MNS}}^{\text{fit}} \sim 1$ to $\cos \delta_{\text{MNS}}^{\text{fit}} \sim -1$.

Figure 11 shows the same contour plots as Fig. 10, but for T2KK with 3.0° OAB at SK and 0.5° OAB at $L = 1000\text{km}$. Significant increase in the $\Delta\chi_{\min}^2$ values at T2KK is clearly seen against those in Fig. 10 for T2KO. Now, the wrong mass hierarchy can be excluded at 5σ level for $\sin^2 2\theta_{\text{RCT}} > 0.08$ (0.09) if the mass hierarchy is normal (inverted). Because the measurement error is dominated by statistics, we find that the 3σ sensitivity of T2KO with 100 kton detector can be archived with a 40 kton detector for T2KK. The CP phase dependence of the T2KK contours is much weaker than that of the T2KO contours, especially for smaller $\sin^2 2\theta_{\text{RCT}}$. This is simply because the matter effect terms at $L \gtrsim 1000\text{ km}$ dominate over the $\sin \delta_{\text{MNS}}$ and $\cos \delta_{\text{MNS}}$ terms, in the correction terms A^e and B^e ; see eq. (23).

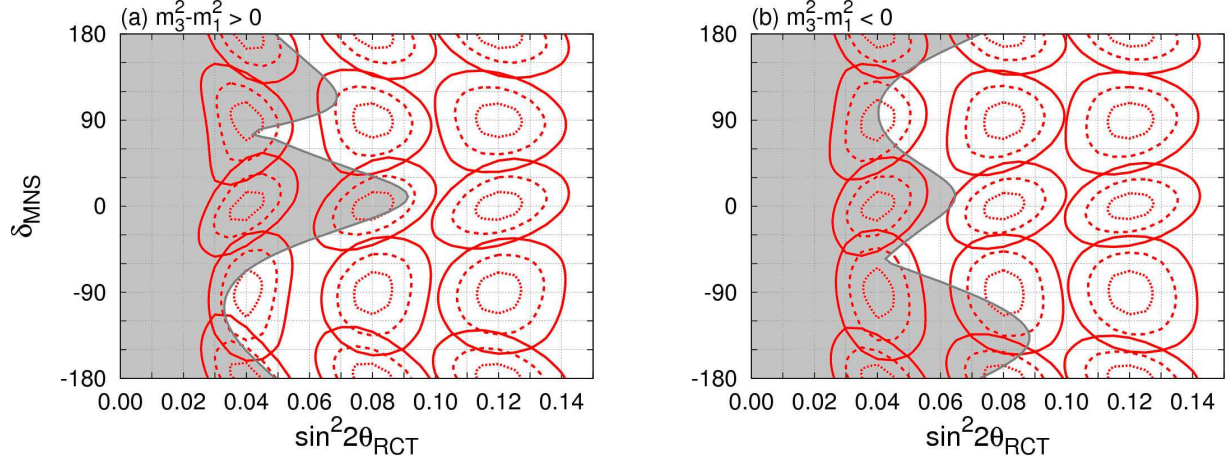


Figure 12: The $\Delta\chi_{\min}^2$ contour plot for the T2KO experiment in the plane of $\sin^2 2\theta_{\text{RCT}}$ and δ_{MNS} when the mass hierarchy is assumed to be normal (left) or inverted (right). Allowed regions in the plane of $\sin^2 2\theta_{\text{RCT}}$ and δ_{MNS} are shown for the combination of 3.0° OAB at SK and 1.4° at Oki Island with 2.5×10^{21} POT each for ν_μ and $\bar{\nu}_\mu$ focusing beams. The input values of $\sin^2 2\theta_{\text{RCT}}$ is 0.04, 0.08, and 0.12 and δ_{MNS} is 0° , 90° , 180° , and 270° . The other input parameters are given in eqs. (28) and (29). The dotted-lines, dashed-lines, and solid-lines show $\Delta\chi_{\min}^2 = 1, 4, \text{ and } 9$ respectively. The shaded region has “mirror” solutions for the wrong mass hierarchy giving $\Delta\chi_{\min}^2 < 9$.

7 CP phase

In this section, we investigate the measurement of CP phase δ_{MNS} in the T2KO experiment, as compared to the T2KK and T2K₁₂₂ options. In all the cases we adopt 3.0° OAB at SK, which makes the SK contribution to the measurements exactly the same, and assume 2.5×10^{21} POT each for ν_μ and $\bar{\nu}_\mu$ focusing beam.

We show in Fig. 12 the $\Delta\chi_{\min}^2$ contour plots for the T2KO experiment in the plane of $\sin^2 2\theta_{\text{RCT}}$ and δ_{MNS} , when the mass hierarchy is assumed to be normal (left) or inverted (right). The 12 cases are shown in each figure for $\delta_{\text{MNS}} = 0^\circ, 90^\circ, 180^\circ, 270^\circ$, and for $\sin^2 2\theta_{\text{RCT}} = 0.04, 0.08, \text{ and } 0.12$. The other input parameters are given in eqs. (28) and (29). The allowed regions in the plane of $\sin^2 2\theta_{\text{RCT}}$ and δ_{MNS} are inside of the dotted-, dashed-, and solid-contours at $\Delta\chi_{\min}^2 = 1, 4, \text{ and } 9$, respectively. The shaded region has “mirror” solutions for the wrong mass hierarchy giving $\Delta\chi_{\min}^2 < 9$, as shown by the red solid contours in Fig. 10. Since the $\sin^2 2\theta_{\text{RCT}} = 0.04$ input cases are no longer relevant after the measurements eqs. (7) and (8) by DayaBay [17] and RENO[23], respectively, the only parameter regions where we should worry about the mirror solution with the wrong hierarchy are around $\delta_{\text{MNS}} \simeq 0^\circ$ at $\sin^2 2\theta_{\text{RCT}} \simeq 0.08$ for the normal hierarchy, and around $\delta_{\text{MNS}} \simeq -135^\circ$ at $\sin^2 2\theta_{\text{RCT}} \simeq 0.08$ for the inverted hierarchy. Since these regions are near the 3σ boundary, the mirror solutions may be excluded by extending the experimental period or by enhancing the beam power. The $\sin^2 2\theta_{\text{RCT}} = 0.04$ input cases are kept, since they show the independence of the δ_{MNS} measurement error on $\sin^2 2\theta_{\text{RCT}}$ clearly. As explained

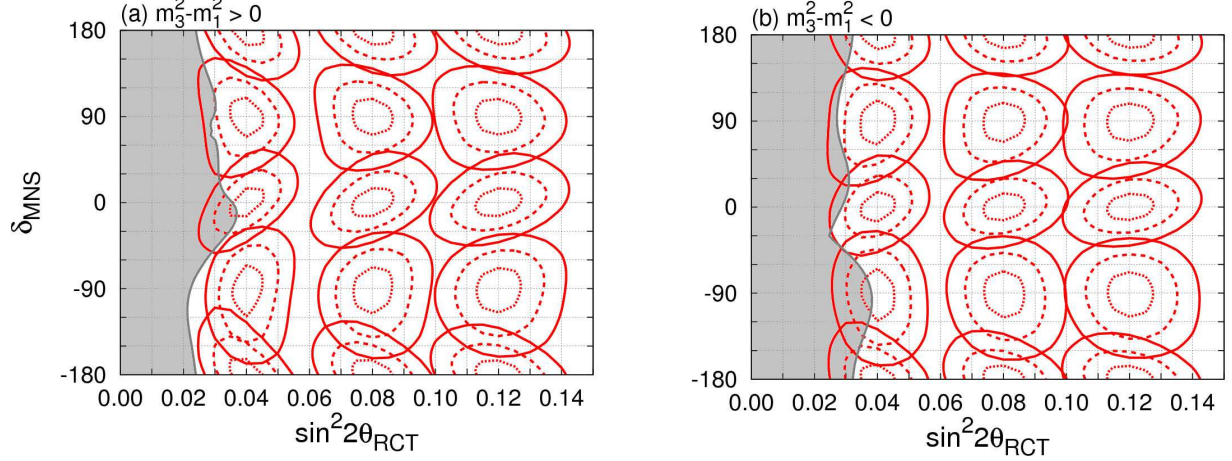


Figure 13: The same as Fig. 12, but for T2KK experiment with 3.0° OAB at SK and 0.5° OAB at $L = 1000\text{km}$.

in Ref.[26, 27], this independence is a consequence of the $1/\sqrt{\sin^2 2\theta_{\text{RCT}}}$ enhancement of the $\sin \delta_{\text{MNS}}$ and $\cos \delta_{\text{MNS}}$ dependencies in A^e and B^e , respectively, in eqs. (23a) and (23b), which cancels precisely the statistical error which is proportional to $\sqrt{\sin^2 2\theta_{\text{RCT}}}$, or the square-root of the $\nu_\mu \rightarrow \nu_e$ and $\bar{\nu}_\mu \rightarrow \bar{\nu}_e$ event numbers.

It is clearly seen that δ_{MNS} can be measured with $\pm 20^\circ$ error for all the 24 cases presented in Fig. 12 (a) and (b). This is essentially because the magnitude of the coefficient of $\sin \delta_{\text{MNS}}$ in the amplitude shift in eq. (23a) and that of $\cos \delta_{\text{MNS}}$ in the phase shift in eq. (23b) are approximately equal. It should be noted that the uncertainty in the $\sin^2 2\theta_{\text{RCT}}$ is dictated by the external constraint with the error of ± 0.01 on the χ^2 function eq. (35). Because of the nearly zero correlation between the errors of δ_{MNS} and $\sin^2 2\theta_{\text{RCT}}$ in Fig. 12, further improvements in the precise measurements of $\sin^2 2\theta_{\text{RCT}}$ will not reduce the errors of δ_{MNS} significantly.

In order to compare the sensitivity of the δ_{MNS} measurement between the T2KO and the T2KK experiments, we show in Fig. 13 the same contours for the T2KK experiment with 3.0° OAB at SK and 0.5° OAB at $L = 1000\text{km}$.

It is clearly seen from the 12 sets of contours, each for normal (left) and inverted (right) hierarchy, that the expected error of δ_{MNS} is $\pm 20^\circ$ for all the combinations, just as for the T2KO experiment shown in Fig. 12. This is remarkable since the event number at a far detector in Korea at $L \simeq 1000$ km is significantly smaller than that in Oki at $L = 653$ km because of the flux which decreases as $1/L^2$ at long distances. This decrease the overall flux is compensated by the wide-band structure of the 0.5° OAB as shown by blue dotted lines in Fig. 4 (a3) and (b3), which enables the far detector in Korea to observe not only the first oscillation peak but also the second one as in Fig. 7. Around the second peak, $|\Delta_{13}/\pi| \sim 3$, and the sensitivity to $\sin \delta_{\text{MNS}}$ and $\cos \delta_{\text{MNS}}$ can be three times higher than the first peak with $|\Delta_{13}/\pi| \sim 1$; see eqs. (23) and (27). In addition, the extended energy range covered by the 0.5° OAB allows the T2KK experiment to measure the phase-shifts B^e and \bar{B}^e accurately, and hence $\cos \delta_{\text{MNS}}$; see eqs. (23b) and (27b). Indeed, we notice in

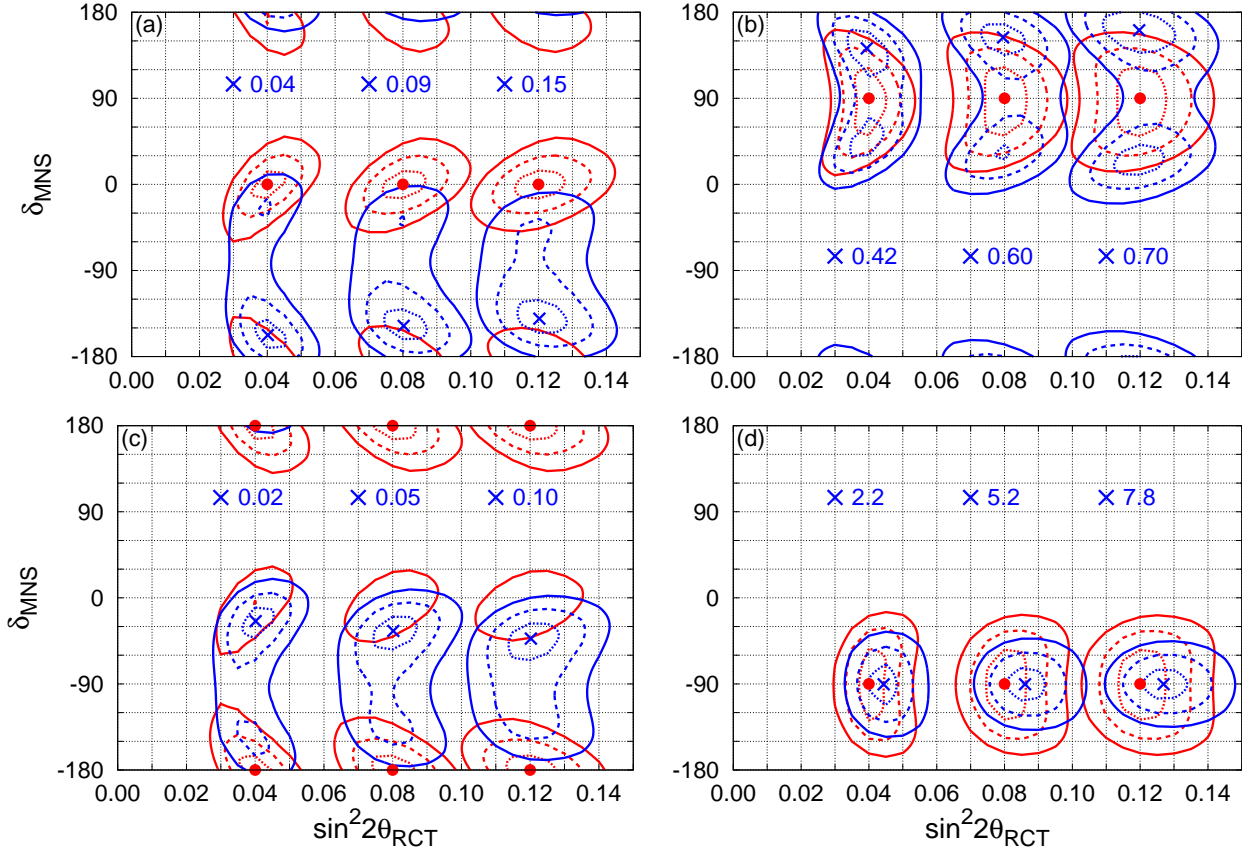


Figure 14: The $\Delta\chi_{\min}^2$ contour plot for the T2K₁₂₂ experiment in the plane of $\sin^2 2\theta_{\text{RCT}}$ and δ_{MNS} when the mass hierarchy is assumed to be normal ($m_3^2 - m_1^2 > 0$). Allowed regions in the plane of $\sin^2 2\theta_{\text{RCT}}$ and δ_{MNS} are shown for experiments with 2.5×10^{21} POT each for ν_μ and $\bar{\nu}_\mu$ focusing beam at 3.0° off-axis angle. The input values of $\sin^2 2\theta_{\text{RCT}}$ are 0.04, 0.08, and 0.12 and δ_{MNS} are 0° (a), 90° (b), 180° (c), and 270° (d). The other input parameters are listed in eqs. (29) and (28). The red dotted-lines, dashed-lines, and solid-lines show $\Delta\chi_{\min}^2 = 1, 4,$ and 9 contours, respectively, when the right mass hierarchy is assumed in the fit, whereas the blue contours give $\Delta\chi_{\min}^2$ measured from the local minimum value (shown besides the \times symbol) at the cross point when the wrong hierarchy is assumed in the fit.

Fig. 13 (a) and (b) that the error of δ_{MNS} can be as small as $\pm 15^\circ$ when $\delta_{\text{MNS}} = 0^\circ$ or 180° .

Finally in Figs. 14 and 15, we show the allowed regions by the T2K₁₂₂ experiment in the plane of $\sin^2 2\theta_{\text{RCT}}$ and δ_{MNS} for the normal (Fig. 14) and the inverted (Fig. 15) mass hierarchy, when both ν_μ and $\bar{\nu}_\mu$ focusing beam at 3.0° off-axis angle are used each with 2.5×10^{21} POT. The four δ_{MNS} cases of 0° (a), 90° (b), 180° (c), 270° (d) are examined for the three $\sin^2 2\theta_{\text{RCT}}^{\text{input}} = 0.04, 0.08, 0.12$, just as in Fig. 12 for T2KO and Fig. 13 for T2KK. The other input parameters are also the same, taken from eqs. (28) and (29). The red dotted-lines, dashed-lines, and solid-lines show $\Delta\chi_{\min}^2 = 1, 4, 9$ contours, respectively, when the right mass hierarchy is assumed in the fit, whereas the blue contours gives $\Delta\chi_{\min}^2$ measured from the local minimum at the blue cross point when the wrong hierarchy is assumed in the fit.

The local minimal value of $\Delta\chi_{\min}^2$ at the blue cross point is given besides the cross

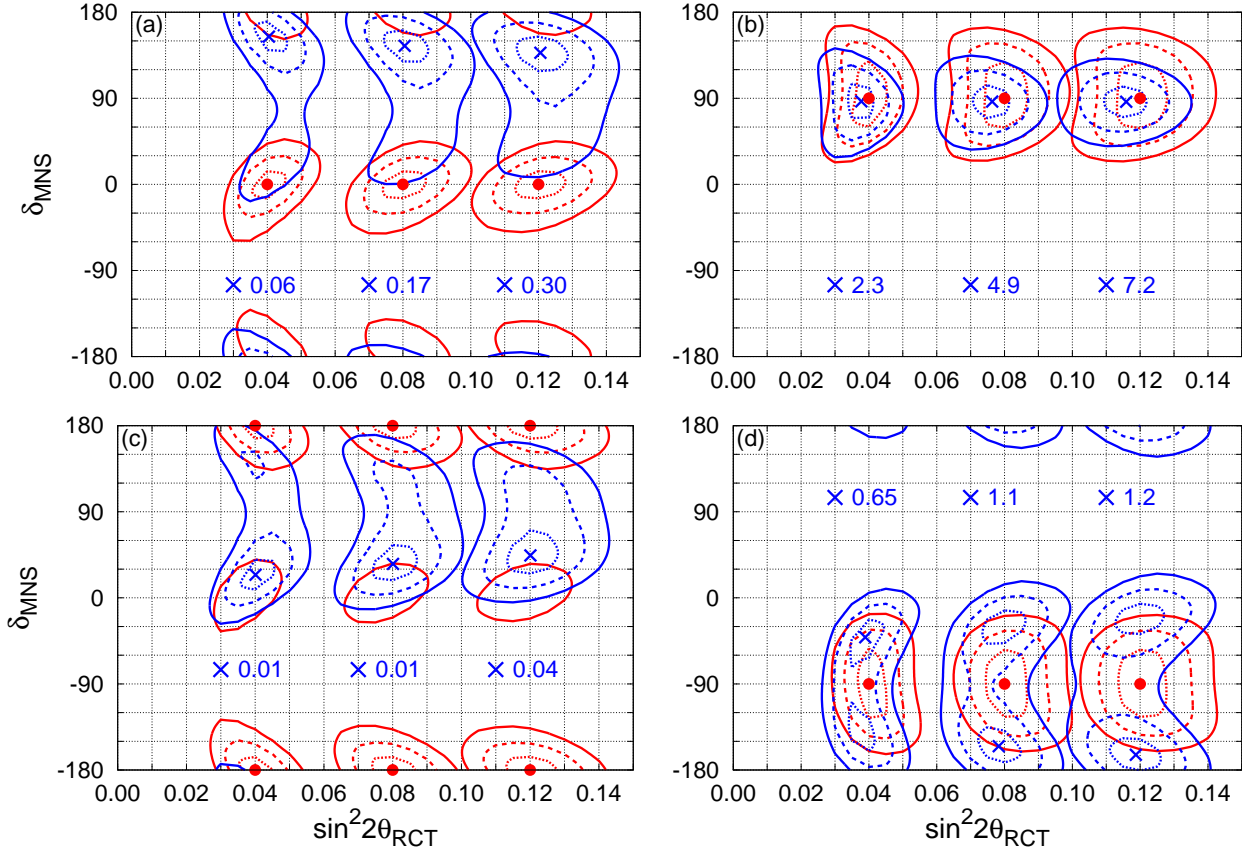


Figure 15: The same as Fig. 14, but for the inverted mass hierarchy ($m_3^2 - m_1^2 < 0$).

mark in the corresponding input $\sin^2 2\theta_{\text{RCT}}$ column. As has been explained in section 6 and shown in Fig. 9, the local $\Delta\chi_{\text{min}}^2$ values are significant only for $\delta_{\text{MNS}} \simeq -90^\circ$ when the hierarchy is normal (Fig. 14 (d)), and for $\delta_{\text{MNS}} \simeq 90^\circ$ when the hierarchy is inverted (Fig. 15 (b)). In order to show the location of the input parameters clearly, we show the global minimal point by the red solid blob for each input parameter case. The global minimum gives $\Delta\chi_{\text{min}}^2 = 0$ in our analysis which ignores fluctuations in the mean number of events in each bin.

We first note that δ_{MNS} can be constrained uniquely around the above two specific cases ($\delta_{\text{MNS}} \simeq -90^\circ$ for $m_3^2 - m_1^2 > 0$, or $\delta_{\text{MNS}} \simeq 90^\circ$ for $m_3^2 - m_1^2 < 0$), since not only the wrong mass hierarchy assumption gives non-negligible local $\Delta\chi_{\text{min}}^2$ as given in Fig. 14 (d) and Fig. 15 (b), but also the wrong hierarchy assumption favors the right δ_{MNS} , with slightly larger (smaller) fitted $\sin^2 2\theta_{\text{RCT}}$ that compensate for the matter effect for the normal (inverted) hierarchy. The 1σ error shown by the red dotted contour is rather large, however, about $\pm 35^\circ$. In all the other cases, the presence of the wrong hierarchy solutions as shown by blue contours significantly reduce the capability of measuring δ_{MNS} with T2K₁₂₂. More importantly, even if we can remove the wrong hierarchy by other experiments such as Nova [34], the next generation reactor neutrino oscillation experiments [47], or by an atmospheric neutrino observation with a huge detector [48, 49], the T2K₁₂₂ experiment with only one baseline length cannot measure δ_{MNS} with high accuracy when $\delta_{\text{MNS}} \simeq \pm 90^\circ$, or suffers from the $\delta_{\text{MNS}}^{\text{fit}} = 180^\circ - \delta_{\text{MNS}}^{\text{input}}$ solution when $\delta_{\text{MNS}} \simeq 0^\circ$ or 180° as can be seen

from the separate red contour islands on the (a) and (c) plots in Figs. 14 and 15.

Throughout the analysis of this and the previous sections we fix the OAB at SK at 3.0° in order to make the SK contributions to all the three experiments T2KO, T2KK and T2K₁₂₂ identical. We find that the performance of T2K₁₂₂ slightly improves if the $2.5^\circ \sim 2.0^\circ$ OAB is adopted instead, mainly because these fluxes are slightly wider (harder) than the 3.0° OAB as shown by red solid curves in Figs. 4 (a1)-(a3), (b1)-(b3).

8 summary

In this paper, we examine physics potential of a one-beam two-detectors neutrino oscillation experiment with an additional 100 kton water Čerenkov detector in Oki Island, which is located along the T2K beam line at the baseline length of $L = 653$ km. Together with Super-Kamiokande (SK) at $L = 295$ km, we can measure neutrino oscillations at two different energies for the same oscillation phase proportional to L/E . We may call this proposal as T2KO (Tokai-to-Kamioka-and-Oki), whose capability has been compared with T2KK (Tokai-to-Kamioka-and-Korea) with $L \simeq 1000$ km for the far detector in Korea, and also with T2K₁₂₂ where the same 100 kton detector is placed at the SK site ($L = 295$ km).

As shown in Fig. 1, since the Oki Island is located in the east side of the T2K beam center, just like the SK, the off-axis angle at Oki Island increases as that at SK increases, as shown in Fig. 3. The off-axis beam (OAB) with 1.4° , 0.9° , and 0.6° from J-PARC can be observed at Oki Island, when the 3.0° , 2.5° , and 2.0° OAB reaches at SK, respectively. The neutrino energy of the first oscillation maximum for the $P(\nu_\mu \rightarrow \nu_e)$ and $P(\bar{\nu}_\mu \rightarrow \bar{\nu}_e)$ is between 1.0 GeV and 1.5 GeV, which depend on the CP phase and the mass hierarchy pattern, at $L = 653$ km. Since the ν_μ ($\bar{\nu}_\mu$) beam between 0.6° and 1.4° off-axis angles has significant intensity around these energies, as shown by green dashed lines in the upper six panels in Fig. 4, we expect that the T2KO experiment can be sensitive to the neutrino mass hierarchy and the CP phase, just like the T2KK experiment [24], [26]-[30].

For a detector of 100 kton fiducial volume and 2.5×10^{21} POT exposure each for both ν_μ and $\bar{\nu}_\mu$ beams, we find that the T2KO experiment can determine the mass hierarchy pattern at 3σ level if $\sin^2 2\theta_{\text{RCT}} = 4|U_{e3}|^2(1 - |U_{e3}|^2)$ is larger than 0.09, by observing the e -like CCQE (Charged-Current Quasi Elastic) events; see Fig. 10. This result does not strongly depend on the off-axis angle of the ν_μ ($\bar{\nu}_\mu$) beam at Oki Island, because the neutrino intensity at the first oscillation maximum does not strongly depend on the off-axis angle at Oki Island. The T2KO sensitivity to the mass hierarchy is about $1/3$ (in $\Delta\chi_{\text{min}}^2$) of the T2KK experiment with the optimum OAB combination of 3.0° at SK and 0.5° at a far detector in Korea with the baseline length around 1000 km. This is because the factor of two higher sensitivity of the T2KK over the T2KO experiment as shown by eqs. (24) and (25), which should give a factor of 4 in $\Delta\chi_{\text{min}}^2$ is partially compensated by the smaller average flux by a factor of $(653 \text{ km}/1000 \text{ km})^2 \simeq 0.4$ at a far detector in Korea. The sensitivity of the mass hierarchy pattern of the T2K₁₂₂ experiment, where a 100 Kton

detector is added at the SK location, is almost zero, except around $\delta_{\text{MNS}} \sim -90^\circ$ (90°) for the normal (inverted) hierarchy; see Fig. 9.

The CP phase in the MNS (Maki-Nakagawa-Sakata) lepton flavor mixing matrix [19], δ_{MNS} can be measured with $\pm 20^\circ$ error for all the four cases at $\delta_{\text{MNS}} = 0^\circ, \pm 90^\circ$, and 180° , almost independent of the $\sin^2 2\theta_{\text{RCT}}$ values [26, 27] as long as the neutrino mass hierarchy is determined. This is because $\sin \delta_{\text{MNS}}$ can be constrained by the difference between the magnitudes of the oscillation probabilities $P(\nu_\mu \rightarrow \nu_e)$ and $P(\bar{\nu}_\mu \rightarrow \bar{\nu}_e)$ around the oscillation maximum, whereas $\cos \delta_{\text{MNS}}$ can be determined by the oscillation phase around the first oscillation maximum, or the location of the oscillation peak(s); see eqs. (23a) and (27a). The sensitivity to the CP phase, δ_{MNS} , of the T2KO experiment is similar to that of the T2KK experiment, mainly because the smallness of the flux at T2KK is compensated by its capability to measure the second oscillation peak at $|\Delta_{13}/\pi| \sim 3$ when the sensitivity to both $\cos \delta_{\text{MNS}}$ and $\sin \delta_{\text{MNS}}$ is a factor of 3 higher than that around the first peak; see eqs. (23).

The T2K₁₂₂ option, which may be regarded as a first step toward the Hyper-Kamiokande [46], cannot generally determine δ_{MNS} , mainly because it cannot resolve mass hierarchy by itself. Only when $\delta_{\text{MNS}} \simeq -90^\circ$ for the normal hierarchy (see, Fig. 14 (d)) and when $\delta_{\text{MNS}} \simeq 90^\circ$ for the inverted hierarchy (see, Fig. 15 (b)), the constraints for both hierarchy assumptions overlap, and the CP phase can be determined uniquely. Even if the mass hierarchy is determined by other experiments [34], [47]-[49] the sensitivity to δ_{MNS} is rather poor at T2K₁₂₂ as shown in Figs. 14 and 15. This is essentially because of the parameter degeneracy unavoidable in experiments with only one baseline length, such as those between δ_{MNS} and $180^\circ - \delta_{\text{MNS}}$ when $\sin \delta_{\text{MNS}} \simeq 0$.

Acknowledgments

We would like to thank our experimentalist colleagues Y. Hayato, A.K. Ichikawa, T. Kobayashi, and T. Nakaya, from whom we learn about the K2K and T2K experiments. We thank N. Isezaki and M. Komazawa for teaching us about the geophysics measurements in the Sea of Japan, or the East Sea of Korea. We are also grateful to Japanese Coast Guard for showing the detailed geological information around Oki Island. The numerical calculations have been carried out on KEKCC at KEK.

References

- [1] Super-Kamiokande Collaboration, Phys. Lett. **B433**, 9 (1998) [arXiv:hep-ex/9803006]; Phys. Lett. **B436**, 33 (1998); Phys. Rev. Lett. **81**, 1562 (1998) [arXiv:hep-ex/9807003]; Phys. Lett. **B467**, 185 (1999); Nucl. Phys. Proc. Suppl. **77**, 123 (1999) [arXiv:hep-ex/9810001].
- [2] Super-Kamiokande Collaboration, Phys. Rev. **D71**, 112005 (2005) [arXiv:hep-ex/0501064]; Soudan 2 Collaboration, Phys. Lett. **B391**, 491 (1997)

- [arXiv:hep-ex/9611007]; Phys. Rev. **D68**, 113004 (2003) [arXiv:hep-ex/0307069]; MACRO Collaboration, Phys. Lett. **B434**, 451 (1998) [arXiv:hep-ex/9807005]; Phys. Lett. **B566**, 35 (2003) [arXiv:hep-ex/0304037].
- [3] K2K collaboration, Phys. Lett. **B511**, 178 (2001) [arXiv:hep-ex/0103001]; Phys. Rev. Lett. **90**, 041801 (2003) [arXiv:hep-ex/0212007]; Phys. Rev. Lett. **94**, 081802 (2005) [arXiv:hep-ex/0411038]; Phys. Rev. Lett. **96**, 181801 (2006) [arXiv:hep-ex/0603004]; Phys. Rev. **D74**, 072003 (2006) [arXiv:hep-ex/0606032].
- [4] Y. Itow *et al.*, [arXiv:hep-ex/0106019]; see also the JHF Neutrino Working Group's home page, <http://jnusrv01.kek.jp/public/t2k>.
- [5] MINOS Collaboration, Phys. Rev. Lett. **97**, 191801 (2006) [arXiv:hep-ex/0607088]; Phys. Rev. **D76**, 072005 (2007) [arXiv:0706.0437(hep-ex)]; Phys. Rev. **D77**, 072002 (2008) [arXiv:0711.0769(hep-ex)]; Phys. Rev. Lett. **101**, 131802 (2008) [arXiv:0806.2237(hep-ex)].
- [6] Super-Kamiokande Collaboration, Phys. Rev. Lett. **85**, 3999 (2000) [arXiv:hep-ex/0009001]; Phys. Rev. Lett. **97**, 171801 (2006) [arXiv:hep-ex/0607059].
- [7] Homestake Collaboration, Astro. J. **496** 505 (1998); SAGE Collaboration, Phys. Rev. **C 60**, 055801 (1999)[arXiv:astro-ph/9907113]; J. Exp. Theor. Phys. **95** 181 (2002) [Zh. Eksp. Teor. Fiz. **95**, 211 (2002)] [arXiv:astro-ph/0204245]; GALLEX Collaboration, Phys. Lett. **B447**, 127 (1999); Super-Kamiokande Collaboration, Phys. Rev. Lett. **81**, 1158 (1998); Erratum *ibid* **81** 4279, (1998) [arXiv:hep-ex/9805021]; Phys. Rev. **D78**, 032002 (2008) [arXiv:0803.4312(hep-ex)]; GNO Collaboration, Phys. Lett. **B490**, 16 (2000) [arXiv:hep-ex/0006034]; Phys. Lett. **B616**, 174 (2005) [arXiv:hep-ex/0504037]; Borexino Collaboration, Phys. Lett. **B658**, 101 (2008) [arXiv:0708.2251(astro-ph)]; Phys. Rev. Lett. **101**, 091302 (2008) [arXiv:0805.3843(astro-ph)]; arXiv:0808.2868(astro-ph).
- [8] SNO Collaboration, Phys. Rev. Lett. **87**, 071301 (2001) [arXiv:nucl-ex/0106015]; Phys. Rev. Lett. **89**, 011301 (2002) [arXiv:nucl-ex/0204008]; Phys. Rev. Lett. **92**, 181301 (2004) [arXiv:nucl-ex/0309004]; Phys. Rev. **C72**, 055502 (2005) [arXiv:nucl-ex/0502021]; Phys. Rev. **C75**, 045502 (2007) [arXiv:nucl-ex/0610020]; Phys. Rev. Lett. **101**, 111301 (2008) [arXiv:0806.0989 [nucl-ex]]; Phys. Rev. **C82**, 055504 (2010) [arXiv:0910.2984 [nucl-ex]]; arXiv:1109.0763 [nucl-ex].
- [9] The KamLAND collaboration, Phys. Rev. Lett. **90**, 021802 (2003) [arXiv:hep-ex/0212021]; Phys. Rev. Lett. **94**, 081801 (2005) [arXiv:hep-ex/0406035]; Phys. Rev. Lett. **100**, 221803 (2008) [arXiv:0801.4589(hep-ex)]; Phys. Rev. **D83**, 052002 (2011) [arXiv:1009.4771 [hep-ex]].
- [10] The CHOOZ Collaboration, Phys. Lett. **B420**, 397 (1998) [arXiv:hep-ex/9711002]; M. Apollonio *et al.*, Eur. Phys. J. **C27**, 331 (2003) [arXiv:hep-ex/0301017].

- [11] F. Boehm *et al.*, Phys. Rev. Lett. **84**, 3764 (2000) [hep-ex/9912050].
- [12] The MiniBooNE Collaboration, Phys. Rev. Lett. **98**, 231801 (2007) [arXiv:0704.1500(hep-ex)]; arXiv:0707.1115(hep-ex).
- [13] L. Wolfenstein, Phys. Rev. **D17**, 2369 (1978); R.R. Lewis, *ibid.* **D21**, 663 (1980); V. Barger, S. Pakvasa, R.J.N. Phillips, and K. Whisnant, *ibid.* **D22**, 2718 (1980); S.P. Mikheyev and A.Yu. Smirnov, Yad. Fiz. **42**, 1441 (1985) [Sov.J.Nucl.Phys.**42**, 913 (1986)]; Nuovo Cimento **C9**, 17 (1986).
- [14] K. Abe *et al.* [T2K Collaboration], Phys. Rev. Lett. **107**, 041801 (2011) [arXiv:1106.2822 [hep-ex]].
- [15] P. Adamson *et al.* [MINOS Collaboration], arXiv:1108.0015 [hep-ex].
- [16] Y. Abe, *et al.* [The Double-CHOOZ Collaboration], arXiv:1112.6353 [hep-ex].
- [17] F.P. An, *et al.* [The Daya Bay Collaboration], arXiv:1203.1669 [hep-ex].
- [18] LSND Collaboration, Phys. Rev. **C54**, 2685 (1996) [arXiv:nucl-ex/9605001]; Phys. Rev. Lett. **77**, 3082 (1996) [arXiv:nucl-ex/9605003]; Phys. Rev. **C58**, 2489 (1998) [arXiv:nucl-ex/9706006]; Phys. Rev. Lett. **81**, 1774 (1998) [arXiv:nucl-ex/9709006]; A. Aguilar *et al.*, Phys. Rev. **D64**, 112007 (2001) [arXiv:hep-ex/0104049].
- [19] Z. Maki, M. Nakagawa, and S. Sakata, Prog. Theor. Phys. **28**, 870 (1962).
- [20] G.L. Fogli, E. Lisi, A. Marrone, and A. Palazzo, Prog. Part. Nucl. Phys. **57** 742 (2006) [arXiv:hep-ph/0506083]; M. Maltoni, T. Schwetz, M.A. Tortola, and J.W.F. Valle, New J. Phys. **6**, 122 (2004) [arXiv:hep-ph/0405172]; T. Schwetz, M. Tortola, and J.W.F. Valle, New J. Phys. **10**, 113011 (2008) [arXiv:0808.2016(hep-ph)].
- [21] Review of the particle physics, C. Amsler, *et al.*, Phys. Lett. **B667**, 1 (2008); see also the particle data group web site, <http://pdg.lbl.gov/>.
- [22] K. Hagiwara and N. Okamura, Nucl. Phys. **B548**, 60 (1999) [arXiv:hep-ph/9811495].
- [23] S.B. Kim, *et al.* [The RENO Collaboration], arXiv:1204.0626 [hep-ex].
- [24] K. Hagiwara, talk at Fujihara Seminar on Neutrino Mass and Seesaw Mechanism (SEESAW 1979-2004), Tsukuba, Ibaraki, Japan, 23-25 Feb. 2004, Published in Nucl. Phys. Proc. Suppl. **137** 84 (2004) [arXiv:hep-ph/0410229].
- [25] M. Ishitsuka, T. Kajita, H. Minakata, and H. Nunokawa, Phys. Rev. **D72**, 033003 (2005) [arXiv:hep-ph/0504026]; T. Kajita, H. Minakata, S. Nakayama, and H. Nunokawa, *ibid.* **D75**, 013006 (2007) [arXiv:hep-ph/0609286].
- [26] K. Hagiwara, N. Okamura, and K. Senda, Phys. Lett. **B637**, 266 (2006)[arXiv:hep-ph/0504061]; Erratum *ibid.* **B641** 486 (2006).

- [27] K. Hagiwara, N. Okamura, and K. Senda, Phys. Rev. **D76**, 093002 (2007) [arXiv:hep-ph/0607255].
- [28] K. Hagiwara and N. Okamura, JHEP**01**, 022 (2008) [arXiv:hep-ph/0611058].
- [29] K. Hagiwara and N. Okamura, JHEP**0907**, 031 (2009) [arXiv:0901.1517 [hep-ph]].
- [30] K. Hagiwara, N. Okamura, and K. Senda, JHEP**09**, 082 (2011) [arXiv:1107.5857 (hep-ph)].
- [31] K. Hagiwara, P. Ko, N. Okamura, and Y. Takaesu in preparation.
- [32] A. Badertscher, T. Hasegawa, T. Kobayashi, A. Marchionni, A. Meregaglia, T. Maruyama, K. Nishikawa, and A. Rubbia, arXiv:0804.2111 [hep-ph].
- [33] M. Yoshioka, T. Hasegawa, O. Hirabayashi, T. Kaneta, K. Kawakami, N. Kimura, T. Maruyama and K. Nishikawa *et al.*, J. Phys. Conf. Ser. **308**, 012028 (2011).
- [34] D.S. Ayres *et al.* [NOvA Collaboration] [hep-ex/0503053]; G.S. Davies for the NOvA Collaboration arXiv:1110.0112 [hep-ex]; R.B. Patterson for the NOvA Collaboration arXiv:1209.0716 [hep-ex].
- [35] T. Takeda *et al.*, Earth Planets Space, **56**, 1293 (2004).
- [36] Geological Sheet Map 1:500,000 No. 8 TOKYO (2nd ed., 2nd print); Fig. 1 in Ref [44].
- [37] D. Zhao, S. Horiuchi, and A. Hasegawa, Tectonophys. **212** 389 (1992).
- [38] T. Sato *et al.*, Geochem. Geophys. Geosyst. **7**, Q06004, (2006).
- [39] T. Sato *et al.*, Tectonophys. **412**, 159, (2006).
- [40] H.J. Kim *et al.*, Tectonophys. **364**, 25 (2003).
- [41] H.M. Cho *et al.*, Geophys. Res. Lett. **33**, L06307 (2006).
- [42] W.J. Ludwig, J.E. Nafe, and C.L. Drake, *Seismic Refraction, in the sea*, ed. A.E. Maxwell, Wiley-Interscience, New York.
- [43] A.K. Ichikawa, private communication; the flux data for various off-axis angles are available from the web page; <http://www2.yukawa.kyoto-u.ac.jp/~okamura/T2KK/>, some beam profiles are obtained with interpolation by ourselves.
- [44] M. Koike and J. Sato, Mod. Phys. Lett. **A14**, 1297 (1999) [hep-ph/9803212].
- [45] R.A. Smith and E.J. Moniz, Nucl. Phys. **B43**, 605 (1972); Erratum. *ibid* **B101** 547 (1975).
- [46] K. Abe *et al.*, arXiv:1109.3262 (hep-ex).

- [47] S.T. Petcov, M. Piai, Phys. Lett. **B533**, 94 (2002); J.G. Learned, S.T. Dye, S. Pakvasa, and R.C. Svoboda, Phys. Rev. **D78**, 071302 (2008); L. Zhan, Y. Wang, J. Cao, and L. Wen, Phys. Rev. **D78**, 111103 (2008); L. Zhan, Y. Wang, J. Cao, and L. Wen, Phys. Rev. **D79**, 073007 (2009).
- [48] D.J. Koskinen, Mod. Phys. Lett. **A26**, 2899 (2011).
- [49] *see e.g.*, S.T. Petcov and T. Schwetz, Nucl. Phys. **B740**, 1 (2006); R. Gandhi, P. Ghoshal, S. Goswami, P. Mehta, S.U. Sankar, and S. Shalgar, Phys. Rev. **D76**, 073012 (2007); R. Gandhi, P. Ghoshal, S. Goswami, and S.U. Sankar, Phys. Rev. **D78**, 073001 (2008); O. Mena, I. Mocioiu, and S. Razzaque, Phys. Rev. **D78**, 093003 (2008); A. Samanta, Phys. Rev. **D81**, 037302 (2010); G. Giordano, O. Mena, and I. Mocioiu, Phys. Rev. **D81**, 113008 (2010); E. Fernandez-Martinez, G. Giordano, O. Mena, and I. Mocioiu, Phys. Rev. **D82**, 093011 (2010); V. Barger, R. Gandhi, P. Ghoshal, S. Goswami, D. Marfatia, S. Prakash, S.K. Raut, and S.U. Sankar, Phys. Rev. Lett. **109**, 091801 (2012); E.Kh. Akhmedov, S. Razzaque, and A.Yu. Smirnov, arXiv:1205.7071(hep-ph).